

# Theoretical Performance Analysis of InN-Based Double Channel High Electron Mobility Transistors (DHEMTs)

By



**Md. Rejvi Kaysir**

A thesis submitted in partial fulfillment of the requirements for the degree of  
Master of Science in Electrical and Electronic Engineering

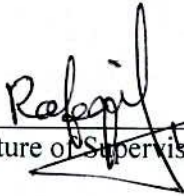


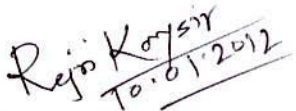
Department of Electrical and Electronic Engineering  
Khulna University of Engineering & Technology  
Khulna 920300, Bangladesh

**January 2012**

## Declaration

This is to certify that the thesis work entitled " *Theoretical Performance Analysis of InN-Based Double Channel High Electron Mobility Transistors (DHEMTs)*" has been carried out by *Md. Rejvi Kaysir* in the Department of *Electrical and Electronic Engineering*, Khulna University of Engineering & Technology, Khulna-920300, Bangladesh. The above thesis work or any part of this work has not been submitted anywhere for the award of any degree or diploma.

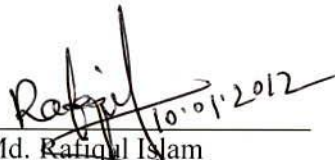
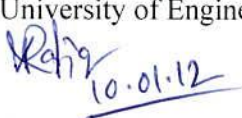

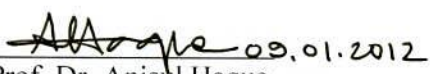
  
Signature of Supervisor 10.01.2012

  
Signature of Student 10.01.2012

## Approval

This is to certify that the thesis work submitted by Md. Rejvi Kaysir entitled "*Theoretical Performance Analysis of InN Based Double Channel High Electron Mobility Transistors (DHEMTs)*" has been approved by the board of examiners for the partial fulfillment of the requirements for the degree of M. Sc. Engineering in the Department of *Electrical and Electronic Engineering*, Khulna University of Engineering & Technology, Khulna-920300, Bangladesh in January 2012.

### BOARD OF EXAMINERS

1.  10.01.2012  
Dr. Md. Rafiqul Islam  
Associate Professor  
Dept. Electrical and Electronic Engineering  
Khulna University of Engineering & Technology  
Chairman  
(Supervisor)
2.  10.01.12  
Prof. Dr. Md. Abdur Rafiq  
Head, Dept. of Electrical and Electronic Engineering  
Khulna University of Engineering & Technology  
Member
3. \_\_\_\_\_  
Prof. Dr. Md. Rafiqul Islam  
Dept. of Electrical and Electronic Engineering  
Khulna University of Engineering & Technology  
Member *Absent*
4.  10.01.2012  
Dr. Mohammad Shaifur Rahman  
Associate Professor  
Dept. of Electrical and Electronic Engineering  
Khulna University of Engineering & Technology  
Member
5.  09.01.2012  
Prof. Dr. Anisul Haque  
Chairperson, Dept. of Electrical & Electronic Engineering  
East West University, Dhaka, Bangladesh  
Member  
(External)

## Acknowledgement

I humbly praise and grateful to ALMIGHTY ALLAH, Who permits me to live and accomplish tasks including the research work being presented in this thesis.

First and foremost, I would like to thank my always inspiring, enthusiastic and very supportive advisor Dr. Md. Rafiqul Islam. He has always been extremely generous with his time, knowledge and ideas and allows me great freedom in this research. I am very proud to have work under his supervision. I offer my sincerest thanks to him for his patience, guidance, illustrious advices, useful suggestions, kind and dynamic supervision throughout the research work. His personal interest, valuable suggestions, most co-operative, constructive thoughtful and affectionate behavior resulted in completion of this thesis.

My appreciation also extends to Prof. Dr. Ashraful G. Bhuiyan, who took me on as my research advisor during my undergraduate time in KUET. He brought me into the fantastic world of semiconductor electronics, and has been always inspired me to strive me the highest level of professionalism. I learned that a qualified researcher should keep open mind and pay persistent effort from him. Without Prof. Bhuiyan's guidance and help, any success in my research career will never be possible.

I am also thankful to Md Sherajul Islam, Assistant professor, Dept. of EEE, for his valuable suggestion and supports during this work. I owe more gratitude to Md Tanvir Hasan than I can express, for supplying me the cutting edge materials.

I am very grateful to have Prof. Dr. Anisul Haque, Chairperson, Department of Electrical & Electronic Engineering, East West University, Dhaka, Bangladesh, in the examination committee. Thanks him for accepting to be on the jury of this dissertation.

I would like to thank the members of the examination committee Prof. Dr. Md Rafiqul Islam, Prof. Dr. Md Abdur Rafiq, Dr. Mohammad Shaifur Rahman to be on the jury of this dissertation.

Lastly but not least, I want to thank my parents for their love, their endless support, and all the sacrifices they have made over the years to provide me with the opportunities to pursue my interest.

## Abstract

### Theoretical Performance Analysis of InN-Based Double Channel High Electron Mobility Transistors (DHEMTs)

In recent years, it has been predicted that InN-based High Electron Mobility Transistors (HEMTs) may be record fast among III-Nitride transistors due to their highly attracting inherent properties. Though the InN-based HEMTs possess superior performance in many aspects, they often suffer from low current densities due to the relatively small number of carriers in the channel. Moreover, carriers in the 2DEG can spill over into the buffer which increases low frequency noise and decreases transconductance. In addition; the spilled over carriers get trapped and thus give rise to slow transient processes and an RF-current collapse, which greatly limits the power performance. To overcome these limitations a Double Channel High Electron Mobility Transistor (DHEMT) made of InGaN/InN/InGaN materials has been considered for better performance. The principal objective of this thesis is to establish a viable concept for the physical One Dimensional (1D) numerical modeling of InGaN/InN/InGaN DHEMTs, to understand the operation mechanism with a focus on main issues improving device performance. At first, a quantum mechanical charge control model based on the self-consistent solution of 1D Schrodinger-Poisson equations is developed. The mobility and velocity-field characteristics are then calculated using Monte Carlo simulation. In order to realize the device performance, a comprehensive quasi-2D model based on the solution of 1D Schrodinger-Poisson-drift diffusion equations is developed. Finally, the dc characteristics i.e. current-voltage and transconductance are obtained from the quasi-2D model for the proposed DHEMTs.

The transport properties provide an ideal platform for the in-depth investigation of InN-based DHEMTs. Among the transport properties electron density and mobility of 2DEGs are two most important concerns. The one dimensional internal electric field and distribution of charges in the channel are demonstrated with the proper material parameters at different bias conditions. The sheet charge density of the 2DEGs is linearly proportional to the number of channels, and reached  $1.25 \times 10^{14} \text{ cm}^{-2}$  for a gate voltage ( $V_g$ ) of 0.4 V at an In composition ( $x$ ) of 0.05 in the  $\text{In}_x\text{Ga}_{1-x}\text{N}$  barrier layer. The highest mobility for the DHEMTs is found to be  $11.5 \times 10^4 \text{ cm}^2\text{V}^{-1}\text{sec}^{-1}$  at  $n_s = 5.2 \times 10^{12} \text{ cm}^{-2}$  at 77 K. The peak velocity of the carrier for the proposed device is found to be  $4.95 \times 10^7 \text{ cm/sec}$  at the field of 57.5 kV/cm. Finally, the maximum channel current is

found to be 1325 mA/mm at a gate voltage of 1.5 V for different values of drain to source voltage for 0.1 $\mu$ m gate length. The calculated value of maximum transconductance is found to be 630 mS/mm. All the results are compared with the conventional InN-based HEMTs and GaN-based DHEMTs and are found excellent performance.

The above analysis strongly suggests that the InGaN/InN/InGaN based DHEMTs have high potential in high frequency and high power applications.

*This work is dedicated to my loved Father, Praiseworthy Mother and Dr Md. Rafiqul Islam  
for guiding me with love and patience*

# Table of Contents

	Page
Title Page.....	i
Declaration.....	ii
Approval.....	iii
Acknowledgement.....	iv
Abstract.....	v
Contents.....	viii
List of Figures.....	xi
List of Table.....	xiii
Nomenclature.....	xiv
<b>Chapter I Introduction</b>	<b>1-7</b>
1.1 Background Information.....	01
1.2 Motivation and Objectives.....	03
1.3 Outline of Dissertation.....	04
References.....	05
<b>Chapter II Theory of III-Nitride DHEMTs</b>	<b>8-25</b>
2.1 Introduction.....	08
2.2 III-Nitride DHEMT Characteristics.....	08
2.2.1 Spontaneous and Piezoelectric Polarizations.....	09
2.2.2 Critical Thickness.....	11
2.2.3 Properties of InN/InGaN/InN Heterostructure.....	13
2.3 Operation Principle of DHEMTs.....	14
2.4 Modeling of DHEMTs.....	16
2.4.1 Equivalent Circuit Based Model.....	16
2.4.2 Physics Based Model.....	17
2.5 Transport Model for III-Nitride DHEMTs.....	18
2.5.1 Drift-Diffusion Model.....	18
2.5.2 Thermodynamic Model.....	18
2.5.3 Hydrodynamic Model.....	19
2.5.4 Impact Ionization Model.....	21
References.....	22



<b>Chapter III Physical One Dimensional Modeling</b>	<b>26-36</b>
3.1 Introduction.....	26
3.2 Device Structure.....	26
3.3 Charge Control Model.....	27
3.3.1 One Dimensional Self Consistent Calculation.....	27
3.3.2 Polarization Effects and Interface Model.....	29
3.3.3 Average Distance of the 2DEGs from Top Heterointerface.....	30
3.4 Quasi-2D Model for Calculation of Current.....	31
3.5 Transconductance Model.....	33
References.....	34
<b>Chapter IV 2DEGs Transport Properties</b>	<b>37-57</b>
4.1 Introduction .....	37
4.2 Carrier Control Characteristics.....	37
4.2.1 Mechanism of Channel Formation and Distribution of Charges in the Channel.....	38
4.2.2 Composition Dependent Potential Profile and Carrier Concentration....	40
4.2.3 Variation of 2DEG Sheet Carrier Density with Gate voltage.....	42
4.2.4 Variation of 2DEG Sheet Carrier Density with Doping Concentration of the Barrier Layer.....	43
4.2.5 Average Distance of 2DEG from Top Heterointerface.....	44
4.3 Mobility Analysis.....	45
4.3.1 Scattering Mechanisms in InN-Based DHEMTs.....	45
4.3.1.1 Dislocation Scattering.....	46
4.3.1.2 Ionized Impurity Scattering.....	47
4.3.1.3 Alloy Disorder Scattering.....	48
4.3.1.4 Interface Roughness Scattering.....	49
4.3.1.5 Phonon Scattering.....	50
4.3.2 Overall Mobility.....	52
4.4 Velocity Field Characteristics.....	53
References.....	55
<b>Chapter V Performance of DHEMTs</b>	<b>58-61</b>
5.1 Introduction.....	58
5.2 Current-Voltage Characteristics.....	58

5.3 Transfer Characteristics.....	59
5.4 Transconductance Characteristics.....	60
References.....	61
<b>Chapter VI Conclusions and Future Work</b>	<b>62-65</b>
6.1 Conclusions.....	62
6.2 Future Work.....	64
References.....	65
<b>Appendix A: List of the Values of Different Parameters of InN Semiconductor.....</b>	<b>66</b>
<b>Publication List.....</b>	<b>67</b>

## List of Figures

Figure No	Description	Page
1.1	Performance of three device technologies--Si BJT, HBT and HEMT- as a function of performance metrics.	02
2.1	Layer structure of InGaN/InN/InGaN based DHEMTs .	10
2.2	Ball and stick model illustrating the crystal structure of (a) wurtzite Ga-polarity and N-polarity GaN and (b) In-polarity [0001] and N-polarity [000-1] wurtzite InN. The surfaces of the In- and N-polarity faces of InN are both shown with In termination.	11
2.3	Critical thickness for the $\text{In}_x\text{Ga}_{1-x}\text{N}/\text{GaN}$ system predicted by the force balance model: comparison between the simplest expression of the $h_c$ , given by Equation 2.10, and a more accurate energy estimation given by Jain et al. based on the derivation by Willis et al.	12
2.4	Calculated sheet charge densities at the upper and lower interfaces caused by spontaneous and piezoelectric polarization for In-face InN/InGa(Al)N/InN heterostructures with In composition of the InGa(Al)N barriers	13
2.5	(a) Schematic cross-section of the DHEMT structure and (b) diagram of the conduction-band edge under external gate voltage, $V_g$ .	15
2.6	Location of 2DEG Sheet Charge densities in the quantum well for the two mode of operation of InGaN/InN/InGaN DHEMT.	16
3.1	Schematic cross section of the proposed InGaN/InN/InGaN based DHEMT.	27
3.2	Schematic representation of the quasi-2D FET model implemented for current calculation in DHEMT	32
4.1	Calculated energy band diagram and electron distribution in the channels for proposed InN based DHEMT at gate bias, $V_g = -0.4 \text{ V}$ .	38

4.2	Calculated energy band diagram and electron distributions in the channels for proposed InN based DHEMT at gate bias, $V_g = 0$ V.	39
4.3	Calculated energy band diagram and electron distribution in the channels for proposed InN based DHEMT at gate bias, $V_g = 0.4$ V.	39
4.4	Variation of conduction band offset at different mole fraction. Inset: A closer view of $\text{In}_x\text{Ga}_{1-x}\text{N}$ /InN region.	40
4.5	Variation of peak electron concentration at different mole fraction. Inset: A closer view of $\text{In}_x\text{Ga}_{1-x}\text{N}$ /InN region.	41
4.6	Sheet carrier density versus In mole fraction( $x$ ) of top $\text{In}_x\text{Ga}_{1-x}\text{N}$ barrier layer.	42
4.7	Gate voltage dependence sheet charge density with different In content( $x$ ) for the proposed QW-DHEMT.	43
4.8	The variation of sheet charge density with donor concentration of top $\text{In}_x\text{Ga}_{1-x}\text{N}$ barrier layer.	44
4.9	Average distance of the 2DEG from the top heterointerface for the proposed 50nm well width DHEMT.	45
4.10	Scattering processes limiting the 2DEGs mobility in InGaN/InN/InGaN heterostructures at 77K	52
4.11	Total mobility of the 2DEGs in the proposed InN based DHEMT structures at 77K.	53
4.12	Total Velocity-Field Characteristics of the proposed InGaN/InN/InGaN based double channel HEMT.	54
5.1	DC current-voltage characteristics of the the proposed InN-based double channel HEMT for 0.1 $\mu\text{m}$ gate length.	58
5.2	Transfer characteristics of the the proposed InN-based double channel HEMT with $V_{DS} = 4$ V.	59
5.3	Transfer Simulated transconductance ( $G_m$ ) versus $V_{GS}$ at $V_{DS} = 4$ V of the proposed InN-based double channel HEMT.	60

## List of Tables

<b>Table No</b>	<b>Description</b>	<b>Page</b>
3.1	Main Material Parameters of binary III-Nitride Compounds.	31
3.2	Parameters used for the one dimensional calculation	34

## Nomenclature

$C_{13}$	elastic constants
$C_{33}$	elastic constants
$d_b$	Thickness of barrier (nm)
$d_{buff}$	Thickness of buffer layer (nm)
$d_{ch}$	Thickness of channel layer (nm)
$d_{spc}$	Thickness of spacer layer (nm)
$D_n$	Diffusion coefficient
$D(z)$	Displacement field
$e_{31}$	Piezoelectric coefficients
$e_{33}$	Piezoelectric coefficients
$E_c$	Critical electric field (KV/cm)
$E_f$	Fermi energy (eV)
$\Delta E_C$	Conduction band offset (eV)
$f_t$	Cut-off frequency (GHz)
$G_m$	Transconductance (mS/mm)
$h$	Plank's Conatant (J-s)
$I_D$	Drain current (mA/mm)
$K$	Boltzman constant ( $JK^{-1}$ )
$L_G$	Gate length ( $\mu m$ )
$L_0$	Drain or source length ( $\mu m$ )
$L_{gap}$	Spacing between gate to source ( $\mu m$ )
$m_0$	Rest mass of electron (Kg)
$N_D$	Donor concentration ( $cm^{-3}$ )
$N_A$	Acceptor concentration ( $cm^{-3}$ )
$n_s$	Sheet carrier concentration ( $cm^{-2}$ )
$P$	Polarization vector ( $Cm^{-2}$ )
$P_{SP}$	Spontaneous polarization ( $Cm^{-2}$ )
$P_{PZ}$	piezoelectric polarization ( $Cm^{-2}$ )
$q$	Electronic Charge (C)
$T$	Temperature (K)
$V_{DS}$	Drain to source voltage (Volt)

$V_{GS}$	Gate to source voltage (Volt)
$v_s$	Saturation velocity (cmsec <sup>-1</sup> )
$V$	potential (Volt)
$W$	gate width (μm)
$x$	Mole fraction
$y$	Distance along channel (nm)
$z$	Distance along growth direction (nm)
$\phi$	Electric field potential
$\Phi_b$	Schottky barrier height (eV)
$\epsilon$	dielectric constant
$\mu$	mobility (cm <sup>2</sup> V <sup>-1</sup> sec <sup>-1</sup> )

# Chapter I

## Introduction

### 1.1 Background Information

Now-a-days, ultra-high speed circuits are based on heterojunction devices like Heterojunction Bipolar Transistors (HBTs) and High Electron Mobility Transistors (HEMTs). HEMT-based high speed integrated circuit (IC)'s and millimeter-wave, microwave IC's [1] need to be scaled to small dimensions for higher performance. The operation frequency of monolithic ICs has recently been extended well into the millimeter-wave range [2, 3]. Millimeter-wave applications call for active devices with high cut-off frequencies and also large current driving capability. The performance analysis of three transistor technologies- BJT, HBT and HEMT as a function of metrics is shown in Figure 1. Each metric is relevant to performance in a different block of a front end. It can be seen that HEMTs are the most promising devices in the field of ultra high speed microwave and digital electronics due to their high cut-off frequencies and low noise figures.

It has been accepted for a couple of years that III-Nitride based HEMTs are becoming the "toughest transistors yet" because of their capability for unprecedented power performance [10]. On the other hand, a large energy band gap and relatively high effective mass ( $m_e$ ) of electrons may limit a carrier effective drift velocity ( $v_e$ ) in the commonly used gallium nitride (GaN) and gallium arsenide (GaAs) channels. This may hinder the III-Nitride HEMT development toward ultra high frequency range applications. Among III-Nitride materials, InN offers the lowest  $m_e = 0.04-0.11m_0$  (in comparison to  $0.2 m_0$  for GaN) and the highest maximal steady-state drift velocity  $v_{max} \sim 5 \times 10^5$  m/s (in comparison to  $\sim 3 \times 10^5$  m/s for GaN) [11, 12]. Consequently, assuming  $v \sim v_{max}$ , InN-based HEMTs may be record fast among III-Nitride transistors, even though the growth of InN heterostructures is still in the immature stage [13, 14]. In the optimal case (if transit time,  $\tau_{RC}$  is maximally eliminated by, e.g., omitting a dielectric passivation on the device surface [15] and assuming  $f \sim v$ ), it may be speculated that cutoff frequency ( $f$ ) may be improved by up to 50% by replacing the GaN with the InN channel. In addition, the InN-channel HEMTs in terms of speed performance may be at least comparable to GaAs and InP-based HEMTs [17], and this conclusion also follows from the comparison of electron velocities in relevant materials [18]. Theoretical analysis has shown that, for ideal



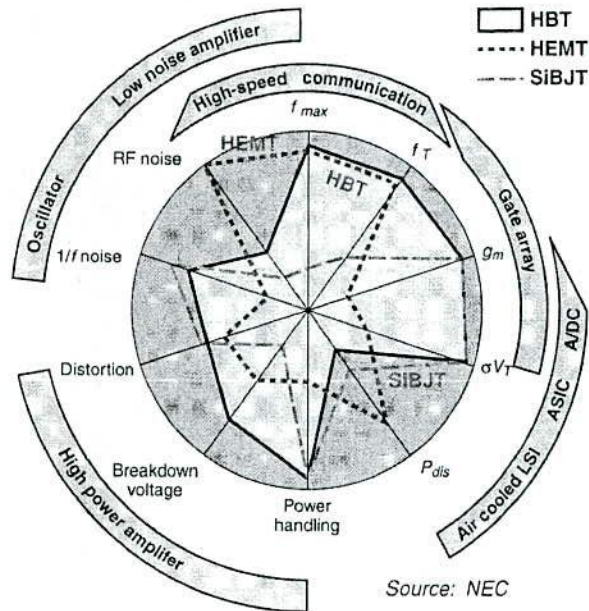


Figure 1.1: Performance of three device technologies--Si BJT, HBT and HEMT- as a function of performance metrics [6].

transistors with gate length ( $L$ )  $0.1 \mu\text{m}$ , by replacing the GaN channel with InN, it can be expected that  $f$  to increase from 480 to 680 GHz [16]. Moreover, low  $m_e$  in the InN channel also gives a prospect for electron non stationary dynamics, and  $f_T$  over 1 THz has been predicted for  $0.1\text{-}\mu\text{m}$  gates in that case [16]. Therefore, in order to meet the future needs of wireless communication systems, research efforts are being put on InN-based HEMTs due to their highly attracting inherent properties.

Though InN-based HEMTs possess superior performance in many aspects, they often suffer from low current densities due to the relatively small number of carriers in the channel. Moreover, carriers in the 2DEG can spill over into the buffer or barrier layers. This spillover increases low frequency noise and decreases transconductance [28]. In addition; the spilled over carriers get trapped and thus give rise to slow transient processes as well as an RF-current collapse, which greatly limits the power performance [26, 27]. To overcome these limitations the sheet carrier density should be increased in the material system. The sheet carrier density can be improved to some extent by increasing the doping in the donor layer at the expense of lower breakdown voltages. A better approach to achieve high current driving capability is by distributing the doping into double donor regions by employing double heterojunctions. In this way double 2DEGs are formed and a high current density can be expected [5]. The HEMTs

which use these double heterojunctions on both sides of the undoped conductive channel is known as Double Channel High Electron Mobility Transistors (DHEMTs). The double heterostructure provides an electron density which is approximately twice than that of conventional single channel HEMT [7, 8] which results in a large output current. It also exhibits a higher transconductance with less degradation over a wide range of gate voltages as compared to the conventional HEMT [9]. Thus, with combined merits of high power and high speed, InN-based DHEMTs have high potential in high frequency and high power applications.

## 1.2 Motivation and Objectives

In the recent years, there have been significant improvements in InN film quality for application to practical devices. Metal organic chemical vapor deposition [19, 20] and molecular beam epitaxy [21, 22] techniques of the growth have been reported to be used to prepare InN films that are 50 nm–10  $\mu$ m thick. Relatively high back ground doping in InN films were observed due to the electron accumulation at the bare surface [21, 23] and at the interface to the GaN buffer [21]. In addition, thin InN films (~10-20 nm) were grown on Ga-polarity GaN [14] or N-polarity InAlN [13] to form InN/GaN and InN/InAlN quantum wells (QWs) respectively. However, there are practically no data on the electrical performance of prepared QWs, and to our knowledge, there are only theoretical calculations on InN-based DHEMTs. Recently, the effect of polarization on carrier confinement and the calculation of 2DEG concentration in InN-based double heterostructure are reported by Hasan et al. [24] which are based on the conventional analytical polarization model. The advances have also been made to investigate the 2DEG properties of InN-based DHEMTs in our previous work [25]. However these papers do not provide clear perception about the physical operation and output performances of InN-based DHEMTs. Therefore, in order to realize the high performance future InN-based DHEMTs, numerical physics based detail device modeling and performance evaluations are urgently required.

In this thesis, InN-based DHEMTs are designed using an undoped InN channel layer which is sandwiched between two n-doped InGaN barrier layers for high performances. Thus, an InGaN/InN/InGaN-based Double Heterostructure Quantum Well (DHQW) system has been considered for demonstration of the device. The principal objective of this thesis is to establish a viable concept for the physical One Dimensional (1D) numerical modeling of InGaN/InN/InGaN DHEMTs, to understand the operation mechanism with a focus on main issues improving device performance. In this research, we have theoretically analyzed the

mechanism of channel formation and the distribution of charges in the channel and the mechanism of carrier control in InGaN/InN/InGaN-based DHQW system. In view of that, 1D numerical self-consistent Schrödinger–Poisson calculations have been developed for the investigations and understanding of energy band diagram and charge distribution in the channel of the proposed device. This model is also applied to investigate the quantum confinement of carriers and the effect of applied gate voltage on the carriers in the quantum well of DHEMTs. We have analyzed the formation and location of 2DEGs at the InGaN/InN and InN/InGaN heterointerfaces by taking into account the spontaneous and piezoelectric polarization effect. In order to realize the device performance, a comprehensive quasi-2D model based on the solution of 1D Schrodinger-Poisson-drift diffusion equations is developed. Finally, this quasi-2D model is extended to calculate the dc output characteristics i.e. current-voltage characteristics and transconductance so as to predict the microwave performance of the device.

### **1.3 Outline of Dissertation**

In the following chapters, InGaN/InN/InGaN DHEMTs are theoretically designed and simulated with one dimensional physics based calculations. The thesis is paying attention on the understanding of the basic operation mechanism of DHEMT devices with a focus on main issues improving device performance. The organization of this thesis is as follows.

In chapter 2 basic properties and design issues of InN-based DHEMTs are reviewed. The intrinsic properties of InGaN/InN and InN/InGaN heterostructures; spontaneous and piezoelectric polarization are investigated. It also quickly reviews the theory of operation and various modeling issues of DHEMTs.

Chapter 3 gives the physics based one dimensional modeling of DHEMTs by self consistently solving Schrödinger equation in conjunction with Poisson's equation to get an insight the physical operation of InN-based DHEMTs. Also, a quasi-2D model is also developed to calculate the current of DHEMT devices.

Chapter 4 describes the results from the 1D self consistent Schrödinger-Poisson calculations. The mechanism of channel formation and distribution of charges in the channel are presented. The effect of various technological parameters on the sheet charge density and the optimization of these parameters are also investigated. The mobility and drift velocity of the proposed device are presented taking into account all relevant scattering and finally the field-velocity characteristics are also presented.

Chapter 5 focuses the dc characteristics of the InN-based DHEMTs. A detail study of the current-voltage characteristics and transconductance are presented to show the device performance.

Chapter 6 contains review of some important terminologies and remarkable findings from our calculated values. It also shows the scope of future works in this area.

#### References:

- [1] T. Suemitsu, H. Yokoyama, Y. Umeda, T. Enoki, Y. Ishii, "High-Performance 0.1- $\mu\text{m}$  Gate Enhancement-Mode InAlAs/InGaAs HEMT's Using Two-Step Recessed Gate Technology," IEEE Trans. Electron Devices, vol. 46, no. 6, pp. 1074-1080, June (1999).
- [2] H. Wang, R. Lai, T. H. Chen, P. D. Chow, J. Velebir, K. L. Tan, D. C. Streit, P. H. Liu, and G. Ponchak, "A monolithic W-band three-stage LNA using 0.1 $\mu\text{m}$  InAlAs/InGaAs/InP HEMT Technology," IEEE MTT-S Int. Microwave Symp. Dig., vol. 2, pp. 519-522, (1993).
- [3] Y. Kwon, D. Pavlidis, T. Brock, and D. C. Streit, "A D-band monolithic fundamental oscillator using InP-based HEMTs," IEEE Trans. Microwave Theory Tech., vol. 41, no. 12, pp. 2236-2344, Dec. (1993).
- [4] J. Lee, H. Yoon, C. Park, and H. Park, "Ultra low noise characteristics of AlGaAs/InGaAs/GaAs pseudomorphic HEMT's with wide head T-shaped gate," IEEE Electron Device Letters, vol. 16, no. 6, pp. 271-273, June (1995).
- [5] Y. Kwon, D. Pavlidis, T. L. Brock, D. C. Streit, "Experimental and Theoretical Characteristics of High Performance Pseudomorphic Double Heterojunction InAlAs/In<sub>0.7</sub>Ga<sub>0.3</sub>As/InAlAs HEMTs," IEEE Trans. Electron Devices, vol. 42, no. 6, pp. 1017-1025, June (1995).
- [6] Kevin F. Brennan, April S. Brown, "Theory of Modern Electronic Semiconductor Devices," New York: Wiley, (2002).
- [7] N. H. Sheng, C. P. Lee, R. T. Chen, D. H. Miller and S. J. Lee, "Multiple-channel GaAs/AlGaAs high electron mobility transistors," IEEE Electron Device Letter, vol. 6, pp. 307-310, June (1985).
- [8] M. Tomizawa, T. Furuta, K. Yokoyama, and A. Yoshi, "Modeling of electron transport in AlGaAs/GaAs/AlGaAs double-heterojunction structures," IEEE Trans. Electron Devives, vol. 36, pp. 2380-2385, Nov. (1989).

- [9] N. H. Sheng, C. P. Lee, R. T. Chen and D. L. Miller, "GaAs/AlGaAs double heterostructure high electron mobility transistors," IEDM Tech. Dig., vol. 30, pp. 352-355, (1984).
- [10] L. F. Eastman and U. K. Mishra, "The toughest transistors yet," IEEE Spectrum, vol. 39, no. 5, pp. 28-33, May (2002).
- [11] V. M. Polyakov and F. Schwierz, "Low-field electron mobility in wurtzite InN," Appl. Phys. Letter, vol. 88, no. 3, pp. 032101, January (2006).
- [12] M. Levinshtein, S. L. Rumyantsev and M. S. Shur, "Properties of Advanced Semiconductor Materials," New York: Wiley, (2001).
- [13] W. Terashima, S. B. Che, Y. Ishitani, and A. Yoshikawa, "Growth and Characterization of AlInN ternary alloys in whole composition range and fabrication on InN/AlInN multiple quantum wells by RF molecular beam epitaxy," Jpn. J. Appl. Phys., vol. 45, no. 21, pp. L539-L542, May (2006).
- [14] E. Dimakis, E. Iliopoulos, M. Kayambaki, K. Tsagaraki, A. Kostopoulos, G. Konstantinidis, and A. Georgakilas, "Growth optimization of electron confining InN/GaN quantum well heterostructure," J. Electron. Mater., vol. 36, no.4, pp. 373-378, Apr. (2007).
- [15] J. Kuzmik, C. Ostermaier, G. Pozzovivo, B. Basnar, W. Schrenk, J. F. Carlin, M. Gonschorek, E. Feltin, N. Grandjean, Y. Douvry, C. Gaquière, J. C. DeJaeger, K. Cico, K. Fröhlich, J. Škriniarová, J. Kovác, G. Strasser, D. Pogany, and E. Gornik, "Proposal and performance analysis of normally-off n<sup>++</sup> GaN/InAlN/AlN/GaN HEMTs with 1-nm-thick InAlN barrier," IEEE Trans. Electron Devices, vol. 57, no. 9, pp. 2144-2154, Sep. (2010).
- [16] B. E. Foutz, S. K. O'Leary, M. S. Shur and L. F. Eastman, "Transient electron transport in wurtzite GaN, InN and AlN," J. Appl. Phys., vol.85, no.11, pp. 7727-7734, Jun. (1999).
- [17] F. Schwierz and J. J. Liou, "RF transistors: Recent developments and road map towards terahertz applications," Solid State Electron., vol. 51, no. 8, pp. 1079-1091, Aug. (2007).
- [18] T. Palacios, "Beyond the AlGaIn/GaN HEMT: New concepts for high-speed transistors," Phys. Stat. Sol. (A), vol. 206, no. 6, pp. 1145-1148, Jun. (2009).
- [19] P. Singh, P. Ruterana, M. Morales, F. Goubilleau, M. Wojdak, J. F. Carlin, M. Ilegems and D. Chateigner, "Structural and optical characterization of InN layers grown by MOCVD," Superlatt. Microstruct., vol. 36, no. 4-6, pp. 537-545, Oct.-Dec. (2004).

- [20] T. Yamaguchi, D. Muto, T. Araki, N. Maeda, and Y. Nanishi, "Novel InN growth method under In-rich condition on GaN/Al<sub>2</sub>O<sub>3</sub> (0001) templates," *Phys. Stat. Sol.(C)*, vol.6, no.S2, pp. S360–S363, Jun. (2009).
- [21] L. F. J. Piper, T. D. Veal, C. F. Mc Conville, H. Lu, and W. J. Schaff, "Origin of the n-type conductivity of InN: The role of positively charged dislocations," *Applied Phys. Lett.*, vol. 88, no. 25, p. 252109, Jun. (2006).
- [22] E. Dimakis, E. Iliopoulos, K. Tsagaraki, A. Adikimenakis, and A. Georgakilas, "Biaxial strain and lattice constants of InN (00010) films grown by plasma-assisted molecular beam epitaxy," *Appl. Phys. Lett.*, vol. 88, no. 19, p. 191918, May (2006).
- [23] C. G. Vande Walle, J. L. Lyons, and A. Janotti, "Controlling the conductivity of InN," *Phys. Stat. Sol. (A)*, vol. 207, no. 5, pp. 1024–1036, May (2010).
- [24] M. T. Hasan, M. M. Rahman, A. N. M. Shamsuzzaman, M. S. Islam, A. G. Bhuiyan, "InN based dual channel high electron mobility transistor," *Proceedings of 4th International Conference on Electrical & Computer Engineering (ICECE-2008)*, 20-22 December, (2008).
- [25] M. T. Hassan, M. R. Kaysir, M. S. Islam, M. R. Islam, A. G. Bhuiyan and Akio Yamamoto, "2DEG properties in InGaN/InN/InGaN-based double channel HEMTs", *Physica Status Solidi (c)*, Vol. 7, No. 7-8, pp. 1997-2000, (2010).
- [26] S. Yagi, M. Shimizu, Y. Yano, A. Ubukata, N. Akutsu, "Current Collapse Characteristic of AlGaIn/GaN MIS-HEMT", *Materials Science Forum*, vol. 600-603, pp. 1333-1336, Sep., (2009).
- [27] T. Mizutani, Y. Ohno, M. Akita, S. Kishimoto, and K. Maezawa, "Study on current collapse in AlGaIn/GaN HEMTs induced by bias stress", *IEEE Trans. on Electron Devices*, vol. 50, pp. 2015-2020, Oct. (2003).
- [28] S. L. Rumyantsev, N. Pala, M. S. Shur and R. Gaska, "Low frequency noise in GaN metal semiconductor and metal oxide semiconductor field effect transistor," *J. Appl Phys.* vol. 80, pp. 310, (2001).

## Chapter II

# Theory of III-Nitride DHEMTs

### 2.1 Introduction

The basic properties and design issues of InGaN/InN/InGaN DHEMTs are presented in this chapter. The basic concept and design of III-Nitride DHEMTs and HEMTs are nearly similar except for the lower barrier layer; HEMTs use only one InGaN (donor layer) barrier layer which form single heterojunction and DHEMTs use two heterojunctions (upper and lower barrier) to enhance the electron confinement in the channel by sandwiching the channel between two InGaN donor layers. Ideally, InN-based DHEMTs should have better performance in terms of power and frequency due to their higher 2DEG density resulting from the higher polarization field, better carrier confinement associated with the higher conduction band discontinuity and higher transconductance due to the thin barrier layer. In the following sections, the operation principles of III-Nitride DHEMTs are investigated and 2DEGs, induced by spontaneous and piezoelectric polarization effects, are reviewed. This chapter ends with the discussion of the various modeling issues and different approaches of transport characterization in DHEMTs.

### 2.2 III-Nitride DHEMT Characteristics

The success of HEMTs is exciting; people start to think about how to make the HEMTs even better. Thus, a narrow band gap material is inserted between two wide band gap materials in HEMTs to form a quantum well structure, which is called Quantum Well Double Heterostructure High Electron Mobility Transistors (QW-DHEMTs). These are also often referred to as Double Channel High Electron Mobility Transistors (DHEMTs). The unique feature of DHEMT is its double heterostructure in which an undoped narrower bandgap material is sandwiched between two higher energy bandgap material allowing carriers to diffuse and form channels. Also due to this modulation doping [18], carriers in the undoped heterointerfaces are spatially separated from the doped region and have extremely high mobility since impurity scattering is absent. The carriers in the heterointerface form a 2DEG since they are confined two dimensionally and are quantized as sheet carrier density. The merit of 2DEG is two-folded: firstly, the separation between ionized impurities and electrons enhanced the mobility; secondly,



the electrons are confined to a thin layer, which improves the carrier modulation efficiency. The better confinement implies higher carrier sheet density and maximum saturation current.

Most of the reported state of the art results of GaN-based and GaAs-based semiconductor devices are from AlGaIn/GaN/AlGaIn [2, 3] and AlGaAs/GaAs/AlGaAs [19] DHEMTs respectively. Although the fundamentals of InN-based DHEMTs are not different from the conventional III-V based DHEMTs, InN-based DHEMTs have distinct properties such as the origin of 2DEG: spontaneous and piezoelectric polarization induced 2DEG [4]. In fact, due to the piezoelectric and spontaneous polarization, InGaIn/InN heterostructure system is able to achieve a 2DEG with sheet carrier concentrations of up to  $\sim 2 \times 10^{14} \text{ cm}^{-2}$  close to the interface [5, 6], which exceeds that observed in other III-V material systems. These high sheet carrier concentrations can be obtained even without intentionally doping the barrier [7]. This effect is much more pronounced in InN based heterostructures when grown on the c-plane than in the case of conventional III-V materials. Furthermore, according to Bernaldini et al. [8], a very large spontaneous polarization charge also exists which must be taken into account in the calculations of the sheet carrier concentration and carefully considered in device design and analysis.

### 2.2.1 Spontaneous and piezoelectric polarizations

The origin of 2DEGs is the spontaneous and piezoelectric polarizations in the case of InGaIn/InN/InGaIn quantum well double heterostructure system. Because of the two distinct polarization mechanisms, 2DEG sheet carrier concentrations of  $\sim 10^{14} \text{ cm}^{-2}$  or higher can be achieved even without intentional doping [6, 9]. Spontaneous polarization is polarization on heterojunction interface at zero strain, which results from net charge of the growth front. Piezoelectric polarization results from the difference between lattice constants at the heterostructure, and thus increases as the strain at the interface increases.

These two polarization effects are quite important in Nitride-based DHEMTs. Figure 2.1 shows device structure of the InGaIn/InN/InGaIn DHEMTs with the locations of 2DEG and polarization charge. The difference in piezoelectric and spontaneous polarization between InGaIn and InN layer determines a fixed 2D charge density at the interface between the two materials. Polarization difference induces a positive charge at the interface and electrons are attracted by this positive charge. The electrons accumulate at the interface and form two conductive channels. The high electric field induced by the interface charge help to form a large channel carrier density and a strong channel confinement. Moreover, the strong electric field



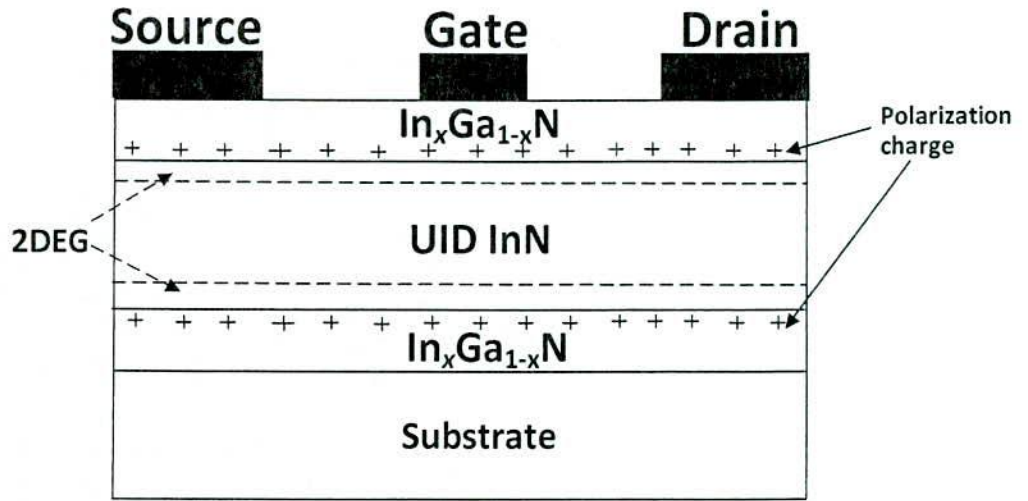


Fig. 2.1 Layer structure of InGaN/InN/InGaN based DHEMTs.

compensates the space charge contribution coming from the ionized donors. The device characteristics are to a great extent decided by the surface termination of the heterostructure. InN grown on sapphire forms a hexagonal wurtzite structure. Along the common growth direction of [0001] or [000-1], atoms are arranged in bilayers. These bilayers are comprised of two closely spaced hexagonal layers, one formed by cations (In atoms) and the other formed by anions (N atoms). If the surface has [0001] polarity, the top position of the [0001] has only In atoms and is referred to as In-face. In contrast, [000-1] polarity has only N at the surface and is referred to as N-face as shown in Fig. 2.2. In-face and N-face surfaces of InN are nonequivalent and different chemically and physically [10, 11]. Strain in the epitaxial layers is primarily caused by the lattice mismatch and thermal expansion coefficients. The epi-layer will be strained or relaxed depending on film thickness. The piezoelectric polarization in the material can be determined by the strain-relaxation profile along the thickness of the epi-layer. As mentioned earlier, the total macroscopic polarization of InN or InGaN layer is the summation of the spontaneous polarization and the piezoelectric polarization. Therefore, if the polarizations are in opposite direction, polarization effect can be reduced. In case of In-face, the spontaneous polarization is pointing towards the substrate. In contrast, the spontaneous polarization of N-faced InGaN/InN heterostructure points to opposite direction [6]. The piezoelectric polarization changes direction depending on the strain; negative for tensile and positive for compressive strained barriers.

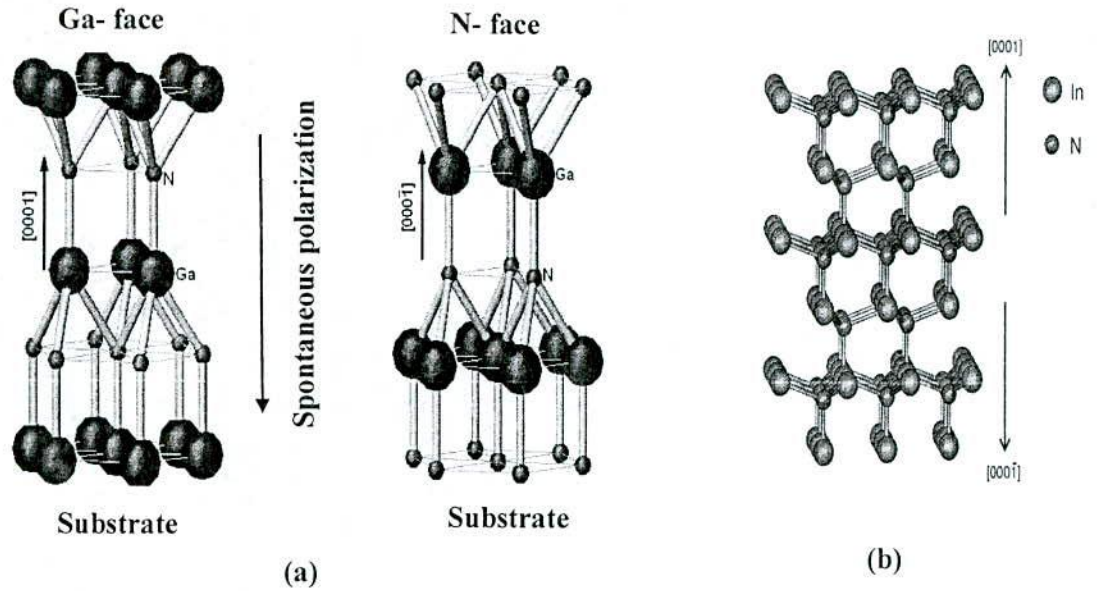


Fig. 2.2 Ball and stick model illustrating the crystal structure of (a) wurtzite Ga-polarity and N-polarity GaN [12] and (b) In-polarity [0001] and N-polarity [000-1] wurtzite InN. The surfaces of the In- and N-polarity faces of InN are both shown with In termination [13].

In order to get high confinement of carrier at the 2DEG, two polarization directions should be same. Thus, compressive strain, InN layer is above InGaN layer, is not adequate for the HEMT operation. In case of the In-face, compressive strain; InN deposited over InGaN, results in minus sheet charge which attract holes at the interface, and the tensile strain; InGaN grown over InN, induces positive sheet charge which attracts electrons. In order to form large sheet carrier concentration of 2DEG at the interface, the tensile strain is required to the In-face, and compressed strain is required to the N-face. Also, for a layer thicker that critical thickness, strain relaxation occurs which leads to the reduction in piezoelectric polarization. Thus, the *polarity* and *critical thickness* of a layer should be taken into account while modeling the III-nitride DHEMT device.

### 2.2.2 Critical thickness

It was shown earlier [20] that a relation between the critical thickness and the strain hardly obey theoretical predictions, and thus, empirical data may provide better estimations. The critical thickness variation with indium content ( $x$ ) in an  $\text{In}_x\text{Ga}_{1-x}\text{N}$  layer on GaN according to the Equation 2.1 for the force balance model is depicted in Figure 2.3 by Holec et.al [21]

$$h_c = \frac{b(1 - \nu \cos^2 \theta)}{8\pi(1 + \nu)|\varepsilon_m| \sin \theta \sin \phi} \ln\left(\frac{h_c}{r_0}\right) \quad (2.1)$$

Where,  $\nu$  is the poisson ratio,  $h_c$  is the critical thickness and  $r_0$  is cutoff radius. The definition of other parameters  $b, \theta, \phi$  and  $\varepsilon_m$  are found in ref. [22]. A more sophisticated model is presented by Willis et al. [20] for taking into account the dislocation energy (see Figure 2.3). The critical thickness decreases with the increase of the In content ( $x$ ) in the  $\text{In}_x\text{Ga}_{1-x}\text{N}$  layer.

It is seen that a 20 nm thick InGaN that is with the InN mole fraction up to 6% to be fully strained on the GaN buffer. Also, the critical layer thickness of GaN/InGaN/GaN double heterostructure system is reported by Reed et al. [25]. If the relaxation mechanism in the proposed InN channel of DHEMTs is similar to that for the reported in the Reference [25], then it is assumed that a thicker InN layer with thickness 50 nm could be grown on the InGaN buffer. Thus, it is concluded that a 50 nm InN thick channel grown on InGaN buffer should be partly relaxed.

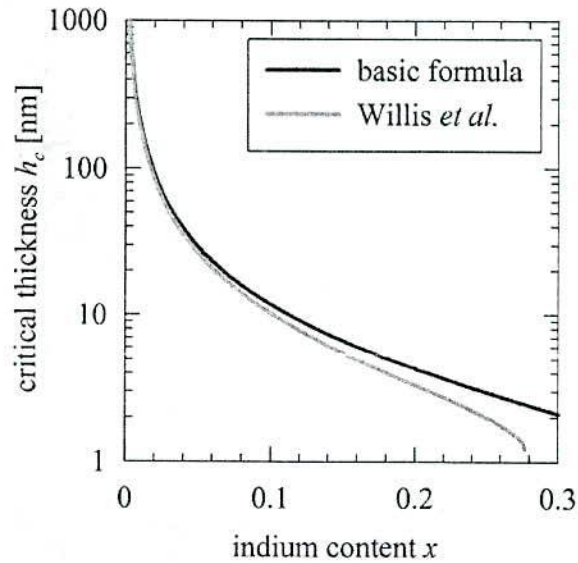


Fig. 2.3 Critical thickness for the  $\text{In}_x\text{Ga}_{1-x}\text{N}/\text{GaN}$  system predicted by the force balance model: comparison between the simplest expression of the  $h_c$ , given by Equation 2.1, and a more accurate energy estimation given by Willis et al. [20].

### 2.2.3 Properties of InN/InGaN/InN Heterostructure

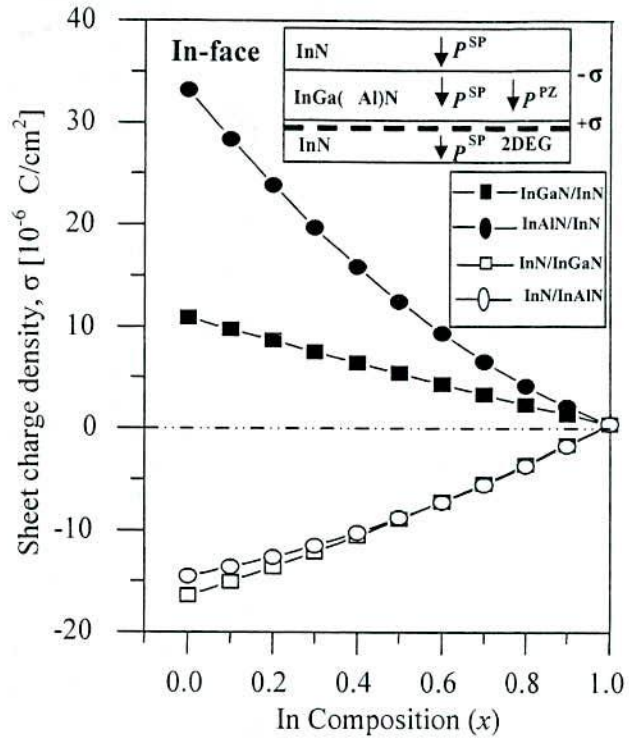


Fig. 2.4 Calculated sheet charge densities at the upper and lower interfaces caused by spontaneous and piezoelectric polarization for In-face InN/InGa(Al)N/InN heterostructures with In composition of the InGa(Al)N barriers [6].

The theoretically calculated sheet charge density from spontaneous and piezoelectric polarization at the lower interface of a In-face InGa(Al)N/InN heterostructure as a function of the alloy composition of the barrier is shown in Fig. 2.4. The calculated values of polarization induced sheet charge densities are found to be positive at the lower interface (InN/InGa(Al)N) and negative at the upper interface (InGa(Al)N/InN) for the In-face heterostructures as shown in the inset. Opposite results are obtained for N-face heterostructure. It is evident that decreasing the In composition improves the sheet carrier density of the 2DEG. However a decrease of In composition results in the reduction of the carrier mobility because of several effects; intersubband scattering, increasing alloy disordering in InGaN, increasing density of interface charges, and larger potential fluctuation due to the surface interface [14].

For the In-face heterostructure, the calculated values of sheet charge densities at lower interface are found to be varied from  $10.37 \times 10^{-06}$  to  $1.97 \times 10^{-06}$  C/cm<sup>2</sup> for InGaN/InN with the variation of In composition from  $x = 0.1$  to  $0.9$ . These calculated sheet charges at the interface are about ten

times higher than other III-V heterostructures [15], thus high polarization induced sheet carrier concentrations may be expected. It has been reported that in the case of InGaN/GaN heterostructures, the polarization can result 2D electron gas (2DEG) and 2D hole gas (2DHG) close to the heterointerface [16] grown on [0001] and [000-1] direction respectively. Recently, Chen et al. [17] reported on an experimental confirmation of a hole accumulation and suggested the acceptors in the InGaN layer to be responsible for this phenomenon.

For the InGaN/InN/InGaN double heterostructure grown in the [0001] direction, it is shown that in an ideally strained and defect-free InN well besides 2DEG at the first interface, a 2DHG is formed at the buried InN/InGaN interface, which is dictated by the piezoelectric polarization in InN [26]. The serious drawback for this structure is that a hypothetical 2DHG with sheet density of  $\sim 10^{12} \text{ cm}^{-2}$  cannot be effectively controlled by the negative gate bias preventing normal DHEMT operations. If the InN channel is partly relaxed, then formation of polarization induced 2DHG is quite improbable [24]. Instead, electron accumulation occurs caused by the interface donors in excess over the negative polarization-induced bound charge. Thus in order to realize the double channel HEMT, the channel should be relaxed or partly relaxed.

As InN has emerged as potentially important semiconductor for use in high-frequency HEMTs [27, 28], however a strong electron accumulation at InN surfaces and interfaces of  $> 10^{13} \text{ cm}^{-2}$ , unintentional n-type doping of  $> 2 \times 10^{17} \text{ cm}^{-3}$  along with a defect-related non-uniform carrier density distribution remain so far the main drawbacks for the studies and fabrication of InN electronic devices [29]. Despite this difficulty, InGaN/InN heterostructure have high potential in terms of high power and high frequency applications and growth control. As fabrication processes progress by optimization, they are expected to lead in breakthrough in III-Nitride based DHEMT technology.

### 2.3 Operation principle of DHEMTs

The schematic and self-explanatory cross-section of the DHEMT structure is shown in Fig. 2.5 (a). The under-gate region of the conduction-band energy diagram for this structure is also shown in Fig. 2.5 (b). Here,  $E_F$  is the position of the Flat-Fermi level, measured from the bottom of the conduction band in the Quantum Well (QW) region. The gate voltage ( $V_g$ ) is applied to gate electrode with respect to source electrode.

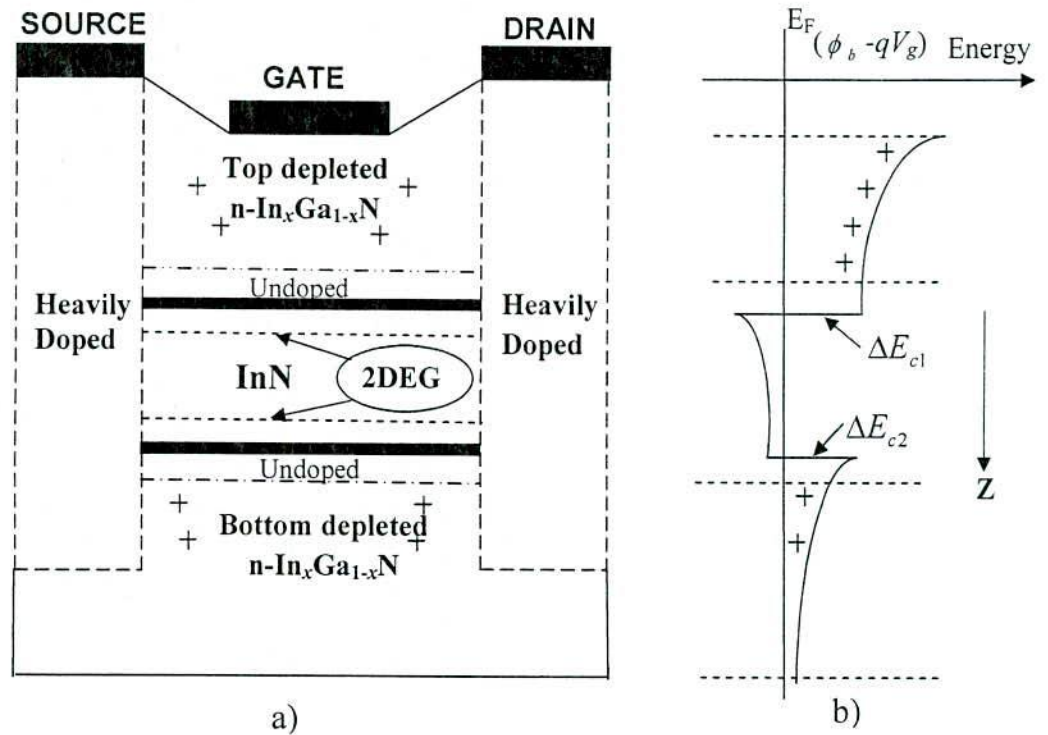


Fig.2.5. (a) Schematic cross-section of the DHEMTs structure. (b) Energy band diagram of the conduction-band edge under external gate voltage  $V_g$ , where  $\phi_b$  is the schottky barrier height.

The upper and lower doped barrier layer forms two heterointerfaces with the undoped channel layer. To reduce the Coulombic coupling between the ionized donors and the 2DEG channels, thin undoped InGaN coulombian spacers are inserted between the QW channel region and n-InGaN layers. As a result of the conduction band discontinuity, two separately potential wells form at the interfaces and charge transfers from the barrier layers to the quantum well in the channel layer. Charge control is achieved by placing a metal Schottky gate on top of the barrier layer that modulates the depletion region in the barrier layer. Below threshold, the sheet charge is fully depleted. Under normal operating conditions, the barrier layer is fully depleted and the channel layer is screened by the formation of the sheet charge at the interfaces. A detailed discussion of the electronic properties of two dimensional systems can be found in the ref. [30]. There are two modes of operation in DHEMTs; Normal HEMT Mode and Inverted HEMT mode [31]. As the gate bias is increased, charge transfer from the barrier layer takes place and only the bottom channel is conducting, where the carriers are confined mainly to the lower interface of the QW. This is known as inverted HEMT mode operation as shown more clearly in Fig. 2.6 (b). The sheet charge density at the bottom channel increases with the increase of gate

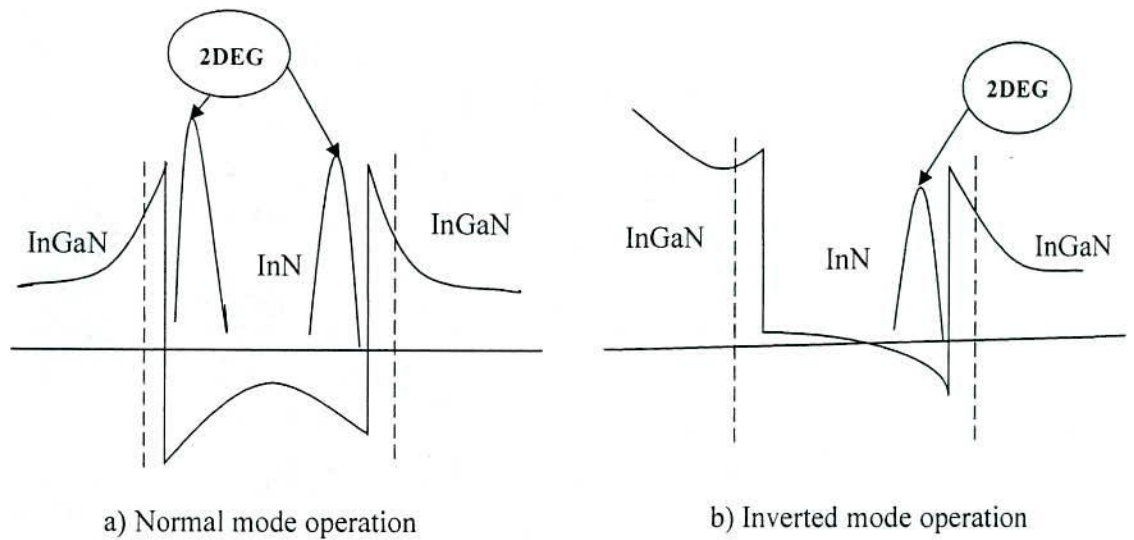


Fig: 2.6 Location of 2DEGs sheet charge densities in the quantum well for the different mode of operation of InGaN/InN/InGaN DHEMT.

voltage until the bottom channel becomes saturated and simultaneously the top channel starts to conduct as shown in Fig. 2.6 (a) is known as normal operation mode. In order to investigate the channel formation and distribution of charges in the channel in DHEMT i.e an accurate description of the charge control in a DHEMT requires a self consistent solution of the Schrödinger and Poisson equations at the Quantum Well. This model is applicable to the situation of a 2DEGs channel with no source-drain voltage and for regions away from the source and drain contacts on 2DEGs.

## 2.4 Modeling of DHEMTs

### 2.4.1 Equivalent Circuit Based Model

Equivalent-circuit-based models are commonly used to investigate large-signal device performance. The DC and RF characteristics of AlGaIn/GaN/InGaIn/GaN Double-Heterojunction HEMTs have been demonstrated by Liu et al. [32]. The output resistance of the D-mode AlGaIn/GaN/In<sub>0.1</sub>Ga<sub>0.9</sub>N/GaN DH-HEMT device was extracted from the S-parameters measured at 2 GHz based on the equivalent circuit model. However, these models require extensive characterization of the device after fabrication, as well as some knowledge of process variation statistics. Equivalent-circuit models also suffer from problems associated with curve-fitting errors and discontinuous or inaccurate high-order derivatives in current and voltage

expressions, leading to inaccurate predictions of the output characteristics and different types of distortion. Also, these models do not provide feedback for the device quality, change of parameters for the output characteristics of the device.

#### **2.4.2 Physics Based Model**

Physical models are becoming increasingly important for active device characterization and design, however, because of the computational demands of most physical models there is usually a compromise between simulation time and accuracy. Physically-based simulation provides advantages over empirical modeling by being predictive and providing insight. In particular, a key advantage is that physical models allow the performance of the device to be closely related to the fabrication process, material properties, and device geometry. This allows performance, yield, and parameter spreads to be evaluated prior to fabrication, resulting in a significant reduction in the design cycle (and cost). Furthermore, since physical models can be embedded in circuit simulations, the impact of device-circuit interaction can be fully evaluated. A further advantage of physical models is that they are generally intrinsically capable of large-signal simulation. For the well-proven physical model, there is no need for an extensive series of measurements since all the data are provided from the process parameters and physical structure of the device. Physical models solve the semiconductor equations explicitly for the device and avoid the problem of ill-defined relationships between equivalent-circuit elements and physical behavior.

In a double-heterojunction (DH) structure, the top and bottom 2DEGs interact. In some cases, this interaction is a source of significant contribution to energy. For a large quantum well (QW), the coupling term adds only a small contribution to energy and generally can be treated as a perturbation. Its effect can, with some cautions, be measured by the overlap integral calculated with the wave functions of the top and bottom channel. For narrow QW systems, such a treatment is not a priori legitimate and to obtain an accurate prediction of the total 2DEG density, at a given gate voltage, self-consistent physics based numerical models [33, 34] must be needed. There are both one dimensional and two dimensional physics based modeling of active device. Two-dimensional models are useful in device analysis [35], and one-dimensional schemes [36], although a popular choice because of their simplicity can be inaccurate.



## 2.5 Transport Model for III-Nitride DHEMTs

### 2.5.1 Drift- Diffusion Model

The direct solution of the full Boltzmann Transport Equation (BTE) is challenging computationally, particularly when combined with field solvers for device simulation. Therefore, for traditional semiconductor device modeling, the predominant model corresponds to solutions of the so-called drift-diffusion equations, which are 'local' in terms of the driving forces (electric fields and spatial gradients in the carrier density), i.e., the current at a particular point in space only depends on the instantaneous electric fields and concentration gradient at that point. The complete drift-diffusion model is based on the following set of equations:

(a) Current Equations

$$J_n = qn \mu_n E + qD_n \nabla n \quad (2.2)$$

$$J_p = qp \mu_p E - qD_p \nabla n \quad (2.3)$$

(b) Continuity equations

$$\frac{\delta n}{\delta t} = \frac{1}{q} \nabla \cdot J_n + U_n \quad (2.4)$$

$$\frac{\delta p}{\delta t} = \frac{1}{q} \nabla \cdot J_p + U_p \quad (2.5)$$

(c) Poisson's equation

$$\nabla \cdot (\epsilon \nabla V) = -[N_D^+ + p - n - N_A^-] \quad (2.6)$$

Where  $U_n$  and  $U_p$  are the net generation-recombination rates. The continuity equations are the conservation laws for the carriers.  $\mu$  is the mobility,  $D$  is the diffusion coefficient, and  $n$  and  $p$  are the charge densities for electron and holes, respectively.

### 2.5.2 Thermodynamic model

The heat generation in the channel is caused by an energy transfer from the electron to the lattice, which is related to inelastic phonon scattering processes of the electron. For this reason, it is necessary to include a thermodynamic (or non-isothermal) model in order to extend the drift-diffusion approach. If the charge carriers are in thermal equilibrium with the lattice, the carrier temperature and the lattice temperature are described by a single temperature. The thermodynamic model is defined by the basic set of partial differential equations and the lattice

heat flow equation. The drift diffusion equation relations are generalized to include the temperature gradient as a driving term [39]:

$$J_n = -qn \mu_n (\nabla \phi_n + P_n \nabla T) \quad (2.7)$$

$$J_p = qn \mu_p (\nabla \phi_p - P_p \nabla T) \quad (2.8)$$

Where,  $P_n$  and  $P_p$  are the absolute thermoelectric powers. To calculate the temperature distribution in the device due to self-heating, the following equation is solved:

$$\begin{aligned} c \frac{\delta T}{\delta t} - \nabla \cdot k \nabla T = & -\nabla \cdot [(P_n T + \phi_n) \bar{J}_n + (P_p T + \phi_p) \bar{J}_p] - (E_c + \frac{3}{2} k_B T) \nabla \cdot \bar{J}_n \\ & - (E_v - \frac{3}{2} k_B T) \nabla \cdot \bar{J}_p + qR(E_c - E_v + 3K_B T) \end{aligned} \quad (2.9)$$

where  $k$  is the thermal conductivity and  $c$  is the lattice heat capacity.  $E_C$  and  $E_V$  are the conduction and valence band energies, respectively, and  $R$  is the recombination rate.  $\phi_n$  and  $\phi_p$  are the potentials.

### 2.5.3 Hydrodynamic model

With continued scaling into the deep submicron regime, neither internal nor external characteristics of state-of-the-art semiconductor devices can be described properly using the conventional drift-diffusion transport model. In particular, the drift-diffusion approach cannot reproduce velocity overshoot and often overestimates the impact ionization generation rates. The Monte Carlo method for the solution of the Boltzmann kinetic equation is the most general approach, but because of its high computational requirements, it cannot be used for the routine simulation of devices in an industrial setting. In this case, the hydrodynamic (or energy balance) model provides a very good compromise. In the hydrodynamic model, the carrier temperatures are assumed to not equal the lattice temperature. Together with basic semiconductor equations, up to three additional equations can be solved to find the temperatures. In general, the model consists of the basic set of PDEs (the Poisson equation and continuity equations) and the energy conservation equations for electrons, holes, and the lattice.

In the hydrodynamic case, current densities are defined as [38, 39]:

$$J_n = q \mu_n (n \nabla E_C + K_B T_n \nabla n + f_n^{td} K_B n \nabla T_n - 1.5 K_B n T_n \nabla \ln m_e) \quad (2.10)$$

$$J_p = q \mu_p (p \nabla E_V + K_B T_p \nabla p + f_p^{td} K_B p \nabla T_p - 1.5 K_B p T_p \nabla \ln m_h) \quad (2.11)$$

where  $E_C$  and  $E_V$  are the conduction and valence band energies, respectively. The first term takes into account the contribution due to the spatial variations of electrostatic potential, electron affinity, and the band gap. The three remaining terms in Eq. 2.10 and Eq. 2.11 take into account the contribution due to the gradient of concentration, the carrier temperature gradients, and the spatial variation of the effective masses  $m_e$  and  $m_h$ .

The energy balance equations read [38, 39]:

$$\frac{\delta W_n}{\delta t} + \nabla \cdot \vec{S}_n = \vec{J}_n \nabla \cdot E_C + \left. \frac{dW_n}{dt} \right|_{coll} \quad (2.12)$$

$$\frac{\delta W_p}{\delta t} + \nabla \cdot \vec{S}_p = \vec{J}_p \nabla \cdot E_V + \left. \frac{dW_p}{dt} \right|_{coll} \quad (2.13)$$

$$\frac{\delta W_L}{\delta t} + \nabla \cdot \vec{S}_L = \left. \frac{dW_L}{dt} \right|_{coll} \quad (2.14)$$

Where the electron heat flux vector ( $\vec{S}_n$ ), hole heat flux vector ( $\vec{S}_p$ ) and lattice heat flux ( $\vec{S}_L$ ) vectors are:

$$\vec{S}_n = -\frac{5r_n}{2} \left( \frac{K_B T_n}{q} \vec{J}_n + f_n^{hf} \hat{k}_n \nabla T_n \right) \quad (2.15)$$

$$\vec{S}_p = -\frac{5r_p}{2} \left( \frac{K_B T_p}{q} \vec{J}_p + f_p^{hf} \hat{k}_p \nabla T_p \right) \quad (2.16)$$

$$\vec{S}_L = -k_L \nabla T_L \quad (2.17)$$

$$\hat{k}_n = \frac{k_B^2 T_n n \mu_n}{q} \quad (2.18)$$

$$\hat{k}_p = \frac{k_B^2 T_p p \mu_p}{q} \quad (2.19)$$

Where  $T_n$ ,  $T_p$  and  $T_L$  represents the electron temperature, hole temperature and lattice temperature respectively. The coefficients  $r$ ,  $f^{td}$ , and  $f^{hf}$  are specified in the Energy Flux, Thermal Diffusion and Heat Flux sections respectively [38]. Different values of the parameters can significantly influence the physical results, such as velocity distribution and possible spurious velocity peaks.

#### 2.5.4 Impact Ionization

Impact ionization and avalanche generation effects are fundamental in a framework where the power applications play a dominant role. Impact ionization has been demonstrated according to the Van Overstraeten-de-Man model [40]. This model is based on the Chynoweth law [37], according to which the impact ionization generation rate for electrons is defined by the following law:

$$G = \alpha n v_{drift} \quad (2.20)$$

where  $n$  is electron concentration,  $v_{drift}$  is drift velocity of electrons, and  $\alpha$  is a field and temperature dependent parameter. The expression used for  $\alpha_{low}$  ( $E < E_0$ ) and for  $\alpha_{high}$  as well as the fitted parameters for electrons, are shown below.

$$\alpha(E) = a \gamma \exp\left(\frac{-b \gamma}{E}\right) \quad (2.21)$$

$$\text{Where, } \gamma = \frac{\tanh(\omega / 2 kT_0)}{\tanh(\omega / 2 kT)} \quad (2.22)$$

In this thesis, all simulations were based on drift-diffusion modeling of the transport characteristics. The model assumes full-ionization, non-degenerate, steady-state and constant temperature. Comparing with the hydrodynamic model, which considers self-heating effects and ballistic transport of the carriers, it is much simpler and faster. Therefore, it is possible to achieve simple and clear identification of key device processes of the DHEMT device.

## References:

- [1] C. Hamaguchi, K. Miyatsuji and H. Hihara, "A proposal of single quantum well transistor (SQWT)-self-consistent calculations of 2D electrons in a quantum well with external voltage," *Jap. J. appl. Phys.*, vol. 23, pp. L132, (1984).
- [2] M. Micovic, P. Hashimoto, Hu Ming, I. Milosavljevic, J. Duvall, P. J. Willadsen, W. S. Wong, P. W. Deelman, M. Jeongs, A. Schmitz, M. J. Delaney, "GaN double heterojunction field effect transistor for microwave and millimeterwave power applications ," *IEDM Technical Digest*, pp. 807-810, (2004).
- [3] Jie Liu, Yugang Zhou, Jia Zhu, Yong Cai, Kei May Lau, Kelvin J. Chen, "DC and RF Characteristics of AlGa<sub>N</sub>/Ga<sub>N</sub>/InGa<sub>N</sub>/Ga<sub>N</sub> Double Heterojunction HEMTs," *IEEE Trans. Electron Devices*, Vol.54, no.1, pp. 2-10, Jan. (2007).
- [4] S. N. Mohammad, A. Salvador, and H. Morkoc "Emerging Gallium Nitride Based Devices", *Proceedings of the IEEE*, Vol. 83, no. 10, Oct. (1995).
- [5] Y. C. Kong, Y. D. Zheng, C. H. Zhou, Y. Z. Deng, "A novel In<sub>x</sub>Ga<sub>1-x</sub>N/InN heterostructure field-effect transistor with extremely high two-dimensional electron gas sheet density," *Solid-State Electronics*, vol. 49, pp. 199, (2005).
- [6] M. T. Hasan, A. G. Bhuiyan, and Akio Yamamoto, "Two dimensional electron gas in InN-based heterostructures: Effects of spontaneous and piezoelectric polarization," *Solid-State Electronics*, vol. 52, pp. 134, (2008).
- [7] F. Sacconi, A. D. Carlo, P. Lugli and Hadis Morkoc, "Spontaneous and Piezoelectric polarization Effects on the Output Characteristics of AlGa<sub>N</sub>/Ga<sub>N</sub> Heterojunction modulation Doped FETs," *IEEE Transaction on Electron Devices*, vol. 48, no. 3, March, (2001).
- [8] F. Bernardini, V. Fiorentini, and D. Vanderbilt, "Spontaneous polarization and piezoelectric constants in III-V nitrides," *Phys. Rev. B*, vol. 56, pp. R10024, (1997).
- [9] O. Ambacher and J. Majewski, C. Smart and J. R. Shealy, "Pyroelectric properties of Al(In)Ga<sub>N</sub>/Ga<sub>N</sub> hetero and quantum well structure," *Journal of Physics: Condense matter*, vol. 14, pp. 3399-4334, (2002).
- [10] O. Ambacher , "Two-dimensional electron gases induced by spontaneous and piezoelectric polarization charges in N- and Ga-face AlGa<sub>N</sub>/Ga<sub>N</sub> heterostructure," *J. appl. Phys.*, vol. 85, no. 6, March (1999).

- [11] Md. Tanvir Hasan, "InN-Based High Electron Mobility Transistors (HEMTs)", Msc Dissertation, KUET, December (2007).
- [12] M. Mehta, O. Jani, C. Honsberg, B. Jampana, I. Ferguson, A. Doolittle, "Modifying PC1D to model spontaneous and piezoelectric polarization in III-V nitride solar cells," 22nd European photovoltaic Solar Energy Conference, Milan, Italy, September 3-7, (2007).
- [13] T. D. Veal, P. D. C. King, P. H. Jefferson, L. F. J. Piper, C. F. McConville, H. Lu, W. J. Schaff, P. A. Anderson, S. M. Durbin, D. Muto, H. Naoi, and Y. Nanishi, "In adlayers on c-plane InN surfaces: A polarity-dependent study by x-ray photoemission spectroscopy," *Phys. Rev (B)*, vol. 76, pp. 075313 (2007).
- [14] F. Bernardini, V. Fiorentini, and D. Vanderbilt, "Spontaneous polarization and piezoelectric constants in III-V nitrides," *Phys. Rev. (B)*, vol. 56, pp. 10024, (1997).
- [15] W. Q. Chen and S. K. Hark, "Strain-induced effects in (111)-oriented InAsP/InP, nGaAs/InP, and InGaAs/InAlAs quantum wells on InP substrates," *J. Appl. Phys.*, vol. 77, pp. 5747-50, (1995).
- [16] C. Wood and D. Jena, "Polarization Effects in Semiconductors," Springer, New York, (2008).
- [17] D. J. Chen, J. J. Xue, B. Liu, H. Lu, Z. L. Xie, P. Han, R. Zhang, Y. D. Zheng, Y. C. Kong, and J. J. Zhou, "Observation of hole accumulation at the interface of an undoped InGaN/GaN heterostructure," *Appl. Phys. Lett.*, vol. 95, pp. 012112, (2009).
- [18] T. Minura, S. Hiyamizu, T. Fujii, and K. Nanbu, "A New Field Effect Transistor with selectively doped GaAs/AlGaAs Heterojunctions," *Jap. J. Appl. Phys.*, 19, L226, (1980).
- [19] M. Tomizawa, T. Furuta, K. Yokoyama, "Modeling of electron transport in AlGaAs/GaAs/AlGaAs Double Heterojunction Structure," *IEEE Trans. on ED*, vol. 36, No. 11, pp. 380-2385, (1989).
- [20] J. R. Willis, S.C. Jain, and R. Bullough, "The energy of an array of dislocations-implications for stain relaxation in semiconductor heterostructures," *Phil. Mag. A*, vol. 62, no.1, pp. 115-129, July (1990).
- [21] David Holic, "Critical thickness calculations for  $\text{In}_x\text{Ga}_{1-x}\text{N}/\text{GaN}$ ," M. Sc Dissertation, University of Cambridge, June (2006).
- [22] J. W. Matthews, A. E. Blakeslee and S. Mader, "Use of misfit strain to remove dislocations from epitaxial thin films", *Thin Solid Films*, vol. 33, pp. 253-266, (1976).

- [23] E. Lioudakis, A. Othonos, E. Iliopoulos, K. Tsagaraki, and A. Georgakilas, "Femtosecond carrier dynamics of  $\text{In}_x\text{Ga}_{1-x}\text{N}$  thin films grown on GaN(0001): Effect of carrier-defect scattering," *J. Appl. Phys.*, vol. 102, no. 7, pp. 073104, Oct. (2007).
- [24] V. Lebedev, V. Polyakov, A. Knübel, R. Aidam, L. Kirste, V. Cimalla, R. Granzner, F. Schwier, and O. Ambacher, "Electron and hole accumulation in InN/InGaN heterostructures", *Phys. Status Solidi C* 8, vol. 2, pp. 485-487, (2011).
- [25] M. J. Reed, N. A. El-Masry, "Critical layer thickness determination of GaN/InGaN/GaN double heterostructures," *Applied Physics Letter*, vol. 77, no. 25, 18 Dec. (2000).
- [26] O. Ambacher, R. Dimitrov, M. Stutzmann, B. E. Foutz, M. J. Murphy, J. A. Smart, J. R. Shealy, N. G. Weimann, W. J. Schaff, and L. F. Eastman, "Role of Spontaneous and Piezoelectric Polarization Induced Effects in Group-III Nitride Based Heterostructures and Devices," *Phys. Status Solidi (B)*, vol. 216, pp. 381, (1999).
- [27] V. Polyakov and F. Schwier, "Low-field electron mobility in wurtzite InN," *Appl. Phys. Lett.*, vol. 88, pp. 032101, (2006).
- [28] J. Wu, "When group-III nitrides go infrared: New properties and perspectives," *J. Appl. Phys.*, vol. 106, pp. 011101, (2009).
- [29] V. Lebedev, V. Cimalla, T. Baumann, O. Ambacher, F. Morales, J. Lozano, and D. Gonzalez, "Effect of dislocations on electrical and electron transport properties of InN thin films. II. Density and mobility of the carriers," *J. Appl. Phys.*, vol. 100, pp. 094903, (2006).
- [30] T. Ando, A. B. Fowler, and F. Stern, "Electronic properties of two-dimensional systems," *Review of Modern Physics*, vol. 54, no. 2, (1982).
- [31] M. Nawaz, G. U. Jensen, "Analytical charge control model for GaAs/AlGaAs-based multiple quantum-well power HEMTs," *Microwave and optical technology letters*, vol. 11, no. 1, January, (1996).
- [32] J. Liu, Y. Zhou, J. Zhu, Y. Cai, K. M. Lau, K. J. Chen, "DC and RF Characteristics of AlGaIn/GaN/InGaIn/GaN Double Heterojunction HEMTs," *IEEE Trans. Electron Devices*, vol.54 , no.1, pp. 2-10, Jan. (2007).
- [33] K. Inoue, H. Sakaki, J. Yoshino, and T. Hotta, "Self-consistent calculation of electronic states in AlGaAs/GaAs/AlGaAs selectively doped double-heterojunction systems under electric fields," *J. Appl. Phys.*, vol. 58, pp. 4277, (1985).

- [34] M. Jaffe, Y. Sekiguchi, J. Singh, D. Pavlidis, and M. Quillec, "A Study Of Charge Control In n- And p-type Lattice Matched And Strained Channel MODFETs With GaAs And InP Substrates," Proc. IEEE/Cornell Conf. Advanced Concepts High Speed Semiconductor Devices Circuits, pp. 70-79, (1987).
- [35] T. Shawki, G. Salmer, and O. El-Sayed, "MODFET 2-D hydrodynamic energy modeling: Optimization of subquarter-micron-gate structures," IEEE Trans. Electron Devices, vol. 37, no. 1, pp. 21-29, January (1990).
- [36] K. Lee, M. S. Shur, T. J. Drummond and H. Morkog, "Parasitic MESFET in (Al, Ga) AdGaAs modulation doped FET's and MODFET characterization," IEEE Trans. Electron Devices, vol. 31, no. 1, pp. 29-35, Jan. (1984).
- [37] A. G. Chynoweth, "Ionization rates for electrons and holes in Silicon", Phys. Rev., vol. 109, no. 5, pp. 1537-1540, (1958).
- [38] DESSIS 9.1 Reference manual, ISE AG, Zurich (Switzerland), (1999), <http://www.ise.ch/>.
- [39] A. Di. Carlo, "GaN-based device simulation and development," PhD dissertation, Univ. of Rome "Tor Vergata", (2009).
- [40] R. Van Overstraeten, H. De Man "Measurement of the ionization rates in diffused silicon p-n junctions," Solid-State Electronics, Vol. 13, issue 5, pp. 583-608, May (1970).



## Chapter III

### Physical One Dimensional Modeling

#### 3.1 Introduction

Simulation studies are necessary at device level for exploring new device designs and concepts. In order to develop advanced InN-based semiconductor devices, a thorough study based on device physics is necessary to allow a better understanding of device operation. However for the device study performed in this thesis, the physics-based approach of charge control study in the InGaN/InN/InGaN double heterostructure is performed by self-consistently solving Schrödinger equation in conjunction with Poisson's equation taking into account the spontaneous and piezoelectric polarization effects. The developed model is employed to study the impact of device performance on various technological parameters.

#### 3.2 Device Structure

The device model considered for this thesis is shown in Fig. 3.1. InN has considered as a channel material. Both side of InN were sandwiched by  $\text{In}_x\text{Ga}_{1-x}\text{N}$  alloy. Due to the lattice mismatch between  $\text{In}_x\text{Ga}_{1-x}\text{N}/\text{InN}$  and  $\text{InN}/\text{In}_x\text{Ga}_{1-x}\text{N}$  heterostructures, there will be intentional stress at the interfaces. Electron will be defused to the lower energy InN layer where they are confined due to the energy barrier at the heterointerfaces. The technique of modulation doping is a perfect means of introducing electrons into the InN channel layer without the adverse effects of donors. The region of the depleted of electrons forms a positive space charge region, which is balanced by the accumulated electrons at the InN heterointerfaces. Even though the electrons and donors are separated spatially, their close proximity allows an electrostatic interaction called Coulombic scattering. By setting the donors away from the interface, Coulombic scattering by donors can be reduced. It has been shown that increasing the spacer layer thickness enhances the electron mobility by reducing Coulombic scattering [1], however it reduces the 2DEG carrier density as well, which is not desired because of the reduction in electron transfer. Therefore a compromise should be made between the donor density in  $n\text{-In}_x\text{Ga}_{1-x}\text{N}$ , conduction band edge discontinuity ( $\Delta E_c$ ), which is controlled by the In content ( $x$ ) in the  $n\text{-In}_x\text{Ga}_{1-x}\text{N}$ , and the thickness of the undoped InGaN spacer layer to maximize both saturation velocity and the electron density of 2DEGs in the undoped InN channel of DHEMTs.

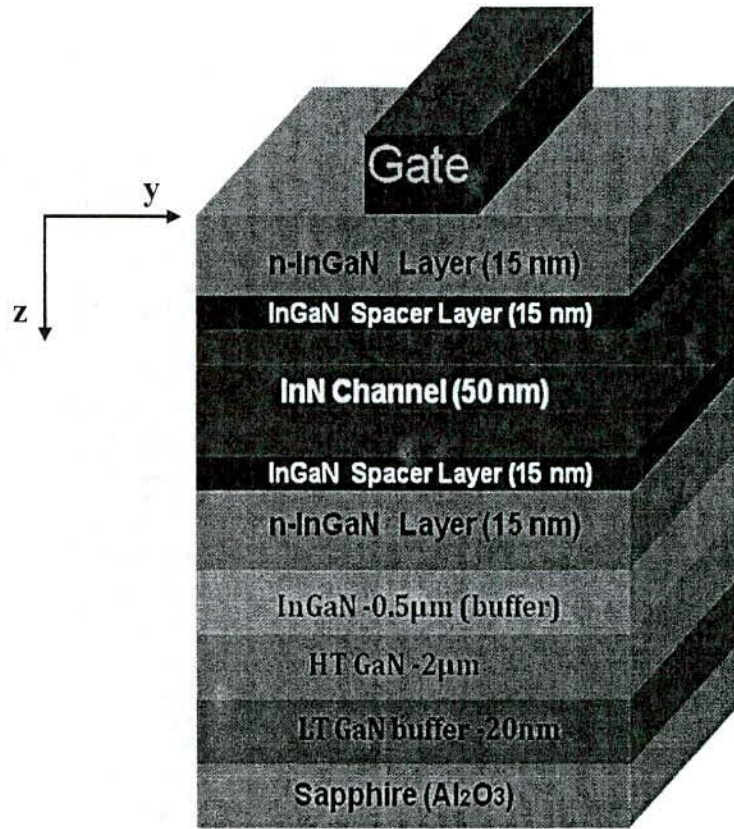


Fig. 3.1 Schematic cross section of the proposed InGaN/InN/InGaN based DHEMTs for one dimensional physical modeling.

### 3.3 Charge Control Model

#### 3.3.1 One Dimensional Self Consistent Calculation

In order to study the mechanism of channel formation and current flow of DHEMTs based on InGaN/InN/InGaN double heterojunction structure, Schrödinger's equation can be used self-consistently coupled with Poisson equation [2, 3].

Within the effective mass theory, Schrödinger's equation takes the form, [4]

$$-\frac{\hbar^2}{2} \frac{d}{dz} \left[ \frac{1}{m(z)} \frac{d}{dz} \right] \varphi_i + [eV(z) + \Delta E(z)] \varphi_i = E_i \varphi_i \quad (3.1)$$

Where,  $m(z)$  is the position dependent effective mass,  $V(z)$  the electrostatic potential,  $\Delta E$  is the band discontinuity at the heterojunction,  $\varphi$  is the electron wave function and  $E$  is the electron energy.

In the Nitride semiconductors grown in the wurtzite structure, due to the presence of spontaneous and piezoelectric polarizations, the displacement field  $D(z)$  is given by Poisson's equation as

$$\frac{d}{dz} D(z) = \frac{d}{dz} \left[ -\varepsilon(z) \frac{d}{dz} V(z) + P(z) \right] = q[N_D^+ + p(z) - n(z) - N_A^-] \quad (3.2)$$

Where,  $\varepsilon(z)$  is the position-dependent dielectric constant,  $P(z)$  the total polarization,  $n$  ( $p$ ) is the electron (hole) charge concentration and  $N_D^+$  ( $N_A^-$ ) is the ionized donor (acceptor) density. The total polarization charge can be written as

$$P = P_{sp} + P_{pz} \quad (3.3)$$

Where,  $P_{pz}$  represents the piezoelectric charge whereas  $P_{sp}$  represents the spontaneous polarization of the InGaN/InN interface. The detail calculation of the total polarization charge ( $P$ ) is presented in the next section 3.3.2.

A self-consistent scheme to solve the above equations by numerical methods has been set up, in which the potential ( $V$ ) is obtained from Eq. 3.2 with an initial guess of the mobile charge concentration, and then inserted into the Schrödinger's equation, (Eq. 3.1) which is solved to obtain the energy levels and wave functions of the system. The new electron charge density is calculated by applying Fermi statistics

$$n(z) = \frac{m(z)K_B T}{\pi \hbar^2} \sum_i |\varphi_i(z)|^2 \ln[1 + e^{(E_F - E_i)/K_B T}] \quad (3.4)$$

Where  $E_F$  is the Fermi level,  $E_i$  is the energy of the  $i$ 'th quantized level,  $T$  is the temperature and  $K_B$  is the Boltzmann constant. The calculated electron density is then plugged into Poisson equation (Eq. 3.2) again and the iteration is repeated until the convergence is achieved. We assume that the Fermi level is constant throughout the structure. This is the reasonable assumption if the gate current is small [7], since the surface Schottky barrier is high enough to prevent the current flow in most of the cases. The Fermi level can be expressed as follows [6]

$$E_F = \frac{n_s}{2D} + \frac{1}{u} \sum_i^u E_i \quad (3.5)$$

Where,  $u$  is the number of sub-band considered,  $D$  is the density of state and  $n_s$  is given below

$$n_s = \frac{mK_B T}{\pi \hbar^2} \sum_i \ln[1 + e^{(E_F - E_i)/K_B T}] \quad (3.6)$$

$$\text{And } D = \frac{qm}{2\pi \hbar^2} \quad (3.7)$$

Here, the simulation is performed numerically by conventional Finite Difference Method (FDM). The boundary condition that we used for the electrostatic potential  $V(z)$  and the electric field  $(-\frac{dV}{dz})$  is that, in the bulk (at the buffer end)  $V=0$  and  $\frac{dV}{dz} = 0$ . While going from one region to another, we use the continuity of potential and electric displacement at the boundary taking into account the different dielectric constants in the two regions which is shown by the Equ. 3.13. The other boundary condition is that at  $z = 0$ ,  $V = V_0$ , a given electrostatic voltage drop across the structure. Knowing the Schottky barrier height ( $\phi_b$ ) and gate voltage ( $V_g$ ) the surface potential  $V_0$  can be calculated. In the simulation region, we assume  $N_A^- = 1 \times 10^{15} \text{ cm}^{-3}$  and  $p(z) = 0$ . The inherent electron accumulation at InN surface due to the effects of surface charge and dislocation densities is not considered. Also, strain has important effects on self-consistent calculations. In this model, strain is incorporated with the piezoelectric polarization effect which is discussed in the next section 3.3.2. But the change of strain induced band gap energy and effective masses are not taking in to account in our calculations. As the higher sub bands have negligible effects [5, 6], only first three sub bands are considered for the calculation.

### 3.3.2 Polarization Effects and Interface Model

There are both linear and non linear models for the computation of polarization charge and it is still not certain which is more suitable [8, 9]. In this thesis paper the linear model is chosen for its physically conceptual simplicity. The calculations have been performed by considering both the spontaneous and piezoelectric polarization charge at the InGaN/InN interface. In principle, polarization charges that form at the metal-InGaN and at the InN/InGaN interface region should be also accounted for. However, the metal-InGaN charge is completely screened by the charges induced on the metal surface and can therefore be neglected. On the other hand, the charges at the InN/InGaN region may have a strong effect. The exact amount of such charge depends, however, on the morphology of the heterojunction. But, a 2DHG is formed at the buried InN/InGaN interface, which is dictated by the piezoelectric polarization in InN which is

discussed in section 2.2.3. The situation is less critical if the InN channel is partly relaxed. In this case, the polarization charge that arises can be completely screened by the residual doping of the lower InGaN layer [10]. On the contrary, if such interface is close to the InGaN/InN heterojunction, the polarization charge can completely deplete the channel. In our simulations we have considered a thick InN partly relaxed channel. Thus, the effect of the polarization charge at the bottom InN/InGaN can be considered completely screened.

The strain induced piezoelectric polarization is expressed by

$$P_{PE}(In_xGa_{1-x}N) = 2 \frac{a(0) - a(x)}{a(x)} \times [e_{31}(x) - e_{33}(x) \frac{C_{13}(x)}{C_{33}(x)}] \quad (3.8)$$

Where,  $a$  is the crystal lattice constant,  $C_{13}$  and  $C_{33}$  are the elastic constants,  $e_{31}$  and  $e_{33}$  are the piezoelectric constants. Spontaneous polarization is also a function of the In mole fraction  $x$ , given by [11]

$$P_{sp}(In_xGa_{1-x}N) = [-0.042x - 0.034(1-x) + 0.037x(1-x)] \text{ C/m}^2 \quad (3.9)$$

$$P_{sp}(InN) = P_{sp}(0) = -0.032 \text{ C/m}^2 \quad [13] \quad (3.10)$$

$$P_{PE}(In_xGa_{1-x}N) = [-0.113(1-x) + 0.0276x(1-x)] \text{ C/m}^2 \quad (3.11)$$

Finally, the sheet charge density at the interface induced by the polarization can be calculated by

$$|\sigma(x)| = |P_{PE}(x) + P_{sp}(x) - P_{sp}(0)| \quad (3.12)$$

For InGaN/InN heterostructure, consideration of the discontinuity of permittivity ( $\epsilon$ ) and the polarization sheet charge at the interface is necessary as shown below:

$$E_{In_xGa_{1-x}N} \epsilon_{In_xGa_{1-x}N} - E_{InN} \epsilon_{InN} = -\sigma \quad (3.13)$$

To calculate the polarization and other material parameters of the compounds, we use Vegard's law and analogous methods to those mentioned in the earlier report [11]. The relevant material parameters are summarized in Table 3.1.

### 3.3.3 Average Distance of the 2DEG from Top Heterointerface

To obtain a high speed DHEMT, one must realize the cutoff frequency ( $f_c$ ). It is mainly determined by carrier velocity and gate capacitance. Thus the average distance from the top heterointerface ( $\tilde{d}_{av}$ ) to the 2DEG is the key factor in addition to the carrier velocity because it is

closely related to the gate capacitance. Smaller  $\tilde{d}_{av}$  is needed for the large gate capacitance.  $\tilde{d}_{av}$  is defined by the following relation [12]

$$\tilde{d}_{av} = \frac{\sum_i^n N_i \int_{-\alpha}^{\alpha} z |\varphi_i(z)|^2 dz}{N_s} \quad (3.14)$$

Where,  $N_i$  is the number of electrons per unit area in the  $i$ 'th subband and  $z$  is the distance perpendicular to the hetero-interface from top hetero interface. These parameters must be taken into account when designing the III-Nitride DHEMT devices.

**Table 3.1**  
**Main Material Parameters of binary III-Nitride Compounds**

Properties of ternary materials can be calculated by  
Applying Vegard's law, e.g,  
 $P_0(A_xB_{1-x}C) = P_0(BC) + x(P_0(AC) - P_0(BC))$

	AlN	GaN	InN
$e_{31} - (C_{31}/C_{33})e_{33}(\text{Cm}^{-2})$	-0.86	-0.86	-0.90
$a_0(\text{Å}^\circ)$	3.112	3.189	3.535
$P_0(\text{Cm}^{-2})$	-0.081	-0.029	-0.032
$E_g(\text{eV})$	6.2	3.39	0.7
$\Delta E_C(\text{to GaN, eV})$	-1.7	-	2.1
$\Delta E_G(\text{to InN, eV})$	-3.8	-2.1	-

### 3.4 Quasi-2D Model for Calculation of Current

A quasi-2D model [4] has been implemented for the calculation of the current-voltage characteristics of the III-nitride DHEMTs. The quasi two-dimensional models are in general based on a solution of the Poisson and current equations using a two-dimensional description of the active channel and on the assumption that the electric field,  $E=E(y)$  is one-dimensional in the channel (see fig. 3.2). This assumption was verified by reference to the results from full two-dimensional models, and allows a considerable reduction of the scale of computational burden [14-17]. This quasi 2D model makes use of the exact value of the sheet charge density in the DHEMT channel, obtained from the self-consistent 1D Schrödinger-Poisson solution discussed above. We use the FET model shown in Fig. 3.2, where the y-axis is along the channel and the

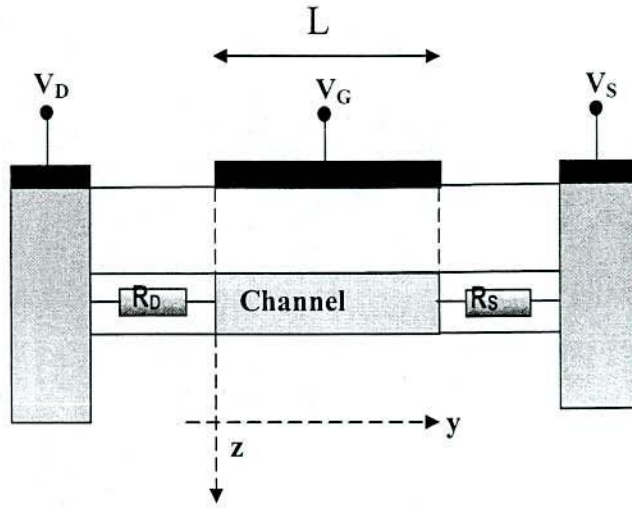


Fig. 3.2 Schematic representation of the quasi-2D FET model implemented for current calculation in DHEMT.

z-axis is along the growth direction. The model also considers the presence of a drain ( $R_D$ ) and source ( $R_S$ ) resistance. When a drain bias ( $V_D$ ) is applied, the potential along the channel may be considered to vary gradually from the source to the drain.

In this situation it is possible to calculate the sheet charge density ( $n_s$ ) in different sections of the channel, provided that one considers the proper potential  $V(y)$  (on the top surface). Since generally  $V_D$  is positive, while  $V_S$  is zero,  $V(y)$  contributes to the channel depletion and the sheet charge density  $n_s$  for the generic  $y$  section of the DHEMT will therefore be:

$$n_s(y) = n_s(V_G - V(y)) \quad (3.15)$$

Since, DHEMT is unipolar device, the diffusion contributions can be neglected from current equation. Thus the source to drain current  $I_{DS}$  is given by:

$$I_{DS} = -qWv(y)n_s(y) \quad (3.16)$$

Where,  $W$  is the gate width and  $v(y)$  the electron mean velocity, taken independent from the transverse coordinate. The drift velocity dependence on the longitudinal electric field is given by:

$$v(y) = \frac{\mu_0 F(y)}{1 + \frac{F(y)}{F_c}} n_s(y) \quad (3.17)$$

Where,  $F(y)$  is the electric field,  $\mu_0$  is the low field mobility and  $F_c = \frac{V_{sat}}{\mu_0}$  is the electric field at saturation. Parasitic components are included explicitly through the value of the drain and source resistance ( $R_D, R_S$ ). For a given value of  $I_{DS}$ , we can calculate the corresponding  $V_D$  by solving Eq. 3.16.

The explicit equation for the current is:

$$I_{DS} = -qW \frac{\mu_0 F(y)}{1 + \frac{F(y)}{F_c}} n_s (V_G - V(y)) \quad (3.18)$$

The numerical solution is based on the discretization of this expression on a number  $N$  of sections, each one with amplitude  $h$ , so that  $Nh=L$ , where  $L$  is the gate length. Given the  $(i-1)$ -th section potential, the  $i$ -th potential is  $V_i=V_{i-1}+F_i h$  where,  $F_i$  is the  $i$ -th section electric field. We have then  $N$  relations:

$$I_{DS} = -qW \frac{\mu_0 F(y)}{1 + \frac{F(y)}{F_c}} n_s (V_G - V_{i-1} - F_i h) \quad (3.19)$$

Since the  $(i-1)$ -th section potential is known from the previous step, this is a non-linear equation in the unknown  $F_i$ . Solving iteratively for all the  $N$  sections, one obtains the value of drain voltage ( $V_D$ ) consistent with the assumed current. Repeating this procedure for a suitable range of values of  $I_{DS}$ , one obtains the set of corresponding  $V_{DS}$  values and builds the device I-V characteristics.

### 3.5 Transconductance Model

Transconductance is one of the most important indicators of device quality for microwave and millimeter wave applications. It is defined as follows

$$G_m = \left. \frac{\partial I_{DS}}{\partial V_{GS}} \right|_{V_{DS}=const} \quad (3.20)$$



**Table: 3.2**  
**Parameters used for the one dimensional calculation**

Parameters	Description	Value
$\phi_b$	Schottky Barrier Height	0.743 eV
T	Temperature	300 K
q	Electronic Charge	$1.6 \times 10^{-19}$ C
$\epsilon_0$	Absolute Permittivity	$8.854 \times 10^{-12}$ F/m
$\epsilon_{10}$	Permittivity of InGaN	11.1 $\epsilon_0$
$m_0$	Rest mass of electron	$9.1 \times 10^{-31}$ kg
$h$	Plank's constant	$6.626 \times 10^{-34}$ J-s
$K_B$	Boltzmann constant	$8.617 \times 10^{-5}$ eVK <sup>-1</sup>
$R_D$	Drain resistance	1 $\Omega$
$R_S$	Source resistance	0.5 $\Omega$
$\mu_0$	Low field mobility	$21 \times 10^2$ cm <sup>2</sup> /Vs

**References:**

- [1] T. Wang, C. H. Hsieh, Hsin-Chu "Numerical analysis of non equilibrium electron transport in AlGaAs/InGaAs/GaAs pseudomorphic MODFETs," IEEE Trans. Electron Devices, vol. 9, pp. 1930–1938, (2002).
- [2] R. Cingolani, A. Botchkarev, H. Tang, and H. Morkoc, "Spontaneous polarization and piezoelectric field in GaN/AlGaN quantum wells: impact on the optical spectra," Phys. Rev. (B), vol. 61, pp. 2711, (2000).
- [3] F. Della Sala, A. Di Carlo, P. Lugli, F. Bernardini, V. Fiorentini, R. Scholz, and J.M. Jancu, "Free-carrier screening of polarization fields in wurtzite GaN/InGaN laser structures," Appl. Phys. Letter, vol. 74, pp. 2002, (1999).

- [4] F. Sacconi, A. DiCarlo, P. Lugli, and H. Morkoc, "Spontaneous and piezoelectric polarization effects on the output characteristics of AlGaIn/GaN heterojunction modulation doped FETs," *IEEE Trans. Electron Devices*, vol. 48, pp. 450-457, March (2001).
- [5] B. Vinter, "Subbands and charge control in a two-dimensional electron gas field-effect transistor," *Appl. Phys. Letter*, vol. 44, pp. 307, (1984).
- [6] A. Rashmi, A. Kranti, S. Haldar, R. S. Gupta, "An accurate charge control model for spontaneous and piezoelectric polarization dependent two-dimensional electron gas sheet charge density of lattice-mismatched AlGaIn/GaN HEMTs," *Solid-State Electronics*, vol. 46, pp. 621-630, (2002).
- [7] K. Inoue, H. Sakaki, J. Yoshino and T. Hotta, "Self-consistent calculation of electronic states in AlGaAs/GaAs/AlGaAs selectively doped double-heterojunction systems under electric fields," *J. Appl. Phys.*, vol. 58, pp. 4277, (1985).
- [8] O. Ambacher, J. Smart, J. R. Shealy, "Two dimensional electron gases induced by spontaneous and piezoelectric polarization charges in N- and Ga-face AlGaIn/GaN heterostructures," *J. Appl. Phys.*, Vol. 85, no.6, pp. 3222, (1999).
- [9] V. Fiorentini, F. Bernardini, O. Ambacher, "Evidence for non linear macroscopic polarization in III-V nitride alloy heterostructure," *Appl. Phys. Letter*, vol. 80, no. 7, pp. 1204, (2002).
- [10] V. Lebedev, V. Polyakov, A. Knübel, R. Aidam, L. Kirste, V. Cimalla, R. Granzner, F. Schwier, and O. Ambacher, "Electron and hole accumulation in InN/InGaIn heterostructures," *Phys. Status Solidi (C)*, vol. 8, no. 2, pp. 485-487, (2011).
- [11] M. T. Hasan, A. G. Bhuiyan, A. Yamamoto, "Two dimensional electron gas in InN-based heterostructures: Effects of spontaneous and piezoelectric polarization," *Solid-State Electronics*, vol. 52, no. 1, pp. 134-139, (2008).
- [12] M. Tomizawa, T. Furuta, K. Yokoyama, "Modeling of electron transport in AlGaAs/GaAs/AlGaAs Double Heterojunction Structure," *IEEE Trans. on Electron Device*, vol. 36, no. 11, pp. 2380-2385, (1989).
- [13] F. Bernardini, V. Fiorentini, D. Vanderbilt, "Spontaneous polarization and piezoelectric constants of III-V nitrides," *Phys. Rev. (B)*, vol. 56, no. 16, pp. R10024-7, (1997).

- [14] B. Carnev, "Modeling of a sub micro meter gate field effect transistor including effects of non stationary electron dynamics," J. Appl. Phys., vol. 51, pp. 784-790, (1980).
- [15] A. Cappy, "Noise modeling in sub micrometer gate two dimensional electron-gas field effect transistor," IEEE Trans. Electron Devices, vol. ED-32, pp. 2787-2796, (1985).
- [16] P. A. Sandborn, J. R. East, and G. I. Haddad, "Quasi two-dimensional modeling of GaAs MESFET's," IEEE Trans. Electron Devices, vol. ED-34, pp. 985-991, Apr. (1987).
- [17] C. M. Snowden and R. R. Pantoja, "Quasi two-dimensional modeling MESFET simulation for CAD," IEEE Trans. Electron Devices, vol. ED-36, pp.1564-1573, Sept. (1989).



## Chapter IV

### 2DEGs Transport Properties

#### 4.1 Introduction

Improving device performances requires an understanding of how the mobility and the density of the Two Dimensional Electron Gases (2DEGs) are increased in the material system. In order to investigate the superior transport properties in the InGaN/InN/InGaN based double heterostructure system, a study of charge control is performed by self-consistently solving Schrödinger equation in conjunction with Poisson's equation taking into account the polarization induced charges. A detailed study of the channel formation mechanism and the distribution of charges in the channel are presented. The mobility and drift velocity of the carrier in the proposed device considering relevant scattering mechanism are described at the end of this chapter.

#### 4.2 Carrier Control Characteristics

To get an insight into the physical operation and carrier control mechanism of InN-based DHEMT, a self-consistent charge control model based on one dimensional Schrodinger-Poisson equations is developed to study the performance. This model is applied to investigate the quantum confinement and the formation of channel with the effect of applied gate voltage. The highly dominant effect of spontaneous and piezoelectric polarization is incorporated in the present model to predict the 2DEG sheet charge density at the InGaN/InN and InN/InGaN heterointerfaces more accurately. For the energy levels corresponding to the 2DEG, it is assumed that the 2DEG lies in an asymmetric two opposed triangular potential well, with the first three subbands occupied. This assumption is reasonable because most of the electrons are occupied in the first three subbands [1, 2]. This is also verified for the proposed InN based DHEMT structure. In addition to the above simplification we neglect the many-body exchange and correlation effects because of their small contributions [3].

#### 4.2.1 Mechanism of Channel Formation and Distribution of Charges in the Channel

The conduction band energy and carrier concentration for the quantum well, formed by the double heterojunction at the barrier and channel interface, at various gate biases based on numerical simulations are investigated here. The band profile is calculated for In mole fraction of  $x=0.05$  in  $\text{In}_x\text{Ga}_{1-x}\text{N}$  barrier layer at 300K. Here, the doping density is considered to be  $N_d=1 \times 10^{19} \text{ cm}^{-3}$  in the  $\text{In}_x\text{Ga}_{1-x}\text{N}$  barrier layers. A large conduction band offset of 2.2 eV is obtained for the proposed device which ensures better carrier confinement and large sheet charge density at the heterointerfaces [4]. At a gate voltage,  $V_g=-0.4 \text{ V}$  (near threshold) only the bottom channel is conducting, where the carriers are confined mainly to the lower interface of the well as shown in Fig.4.1. The peak charge concentration is found to be as high up to  $7.5 \times 10^{17} \text{ cm}^{-3}$  at this condition. The sheet charge density at the bottom channel increases with the increase of gate voltage (so called inverted HEMT mode) until the bottom channel becomes saturated and simultaneously the top channel starts to conduct as shown in Fig.4.2. Because of the carriers are localized near the bottom heterointerface, smaller gate capacitance is achieved due to the increased separation between metal gate and the 2DEG density.

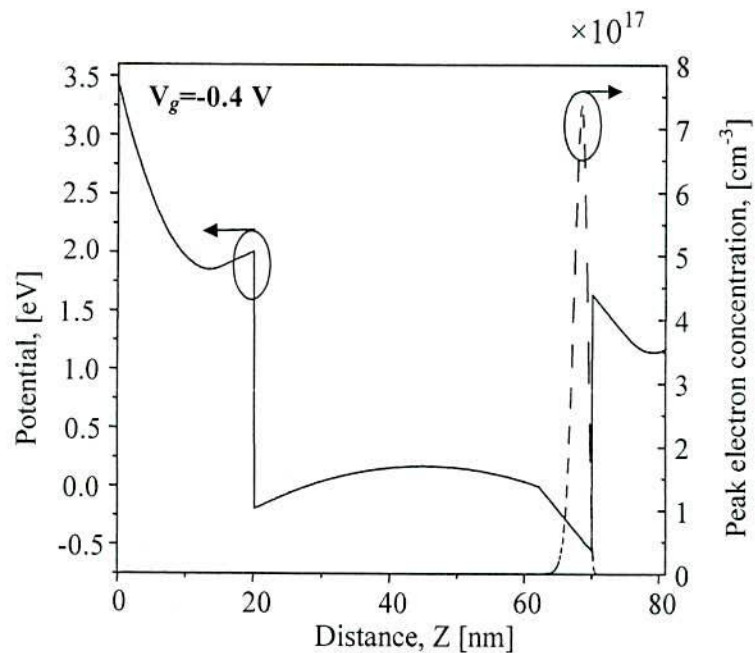


Fig. 4.1 Calculated energy band diagram and electron distribution in the channel for proposed InN based DHEMT at gate bias,  $V_g = -0.4 \text{ V}$ .

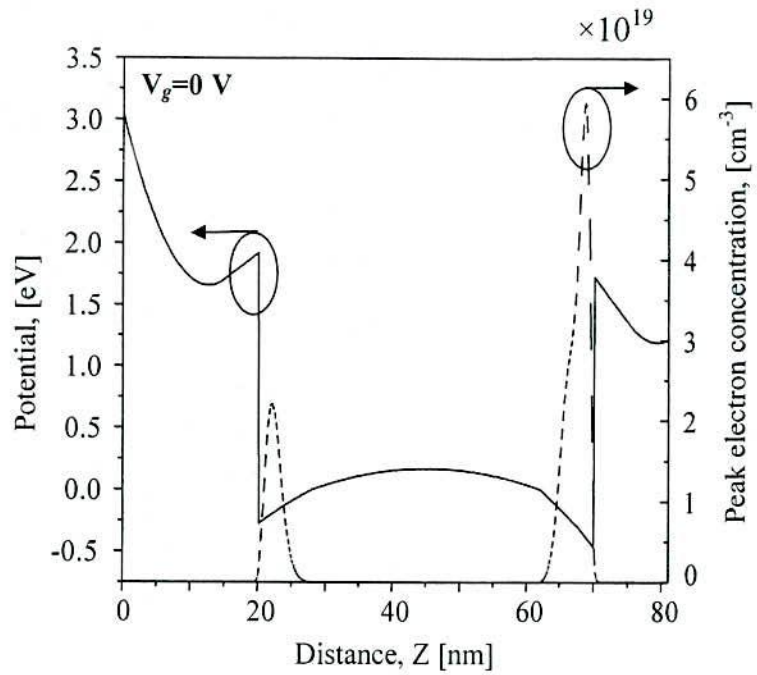


Fig. 4.2 Calculated energy band diagram and electron distributions in the channel for proposed InN based DHEMT at gate bias,  $V_g = 0$  V.

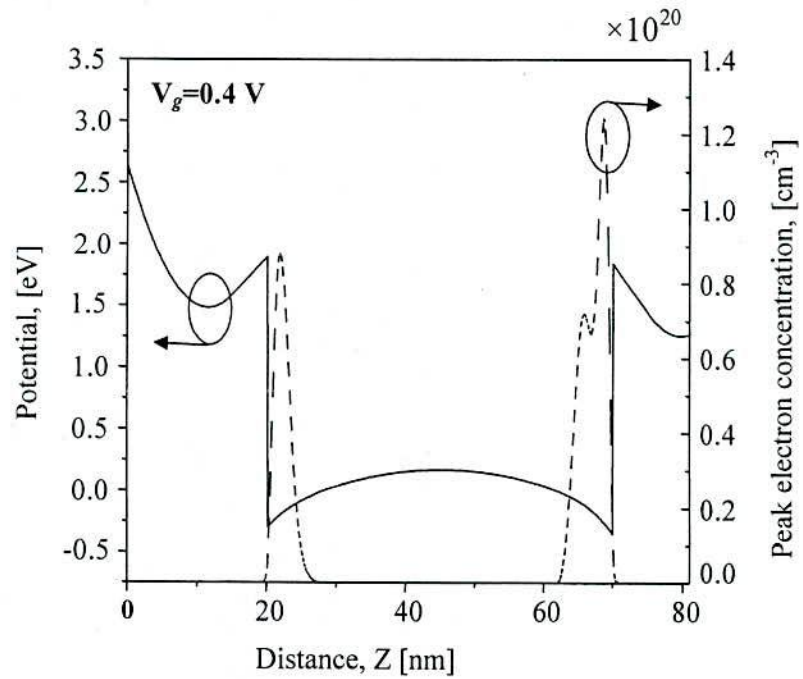


Fig. 4.3 Calculated energy band diagram and electron distributions in the channel for proposed InN based DHEMT at gate bias,  $V_g = 0.4$  V.

The top heterointerface starts to accumulate 2DEG charges at  $V_g=0V$ , which is clearly shown by the emergence of second peak. The peak electron concentration for the bottom and top channel is found to be  $6.1 \times 10^{19} \text{ cm}^{-3}$  and  $2.35 \times 10^{19} \text{ cm}^{-3}$  respectively. At  $V_g=0.4 \text{ V}$ , two clear distinct peaks show the conduction of two channels separately inside the quantum well (see Figure 4.3). The gate capacitance increases due to the decreased distance between sheet charge density and the metal gate. The 2DEG peak electron concentration for bottom channel and top channel is found to be  $1.25 \times 10^{20} \text{ cm}^{-3}$  and  $0.89 \times 10^{20} \text{ cm}^{-3}$  respectively. The calculated total sheet charge density is as high as  $1.25 \times 10^{14} \text{ cm}^{-2}$  in this case.

This high sheet carrier density is due to the quantum confinement effect caused by the large conduction band offset of 2.2 eV and a large polarization induced sheet charge density because of the lattice mismatch between InGaN barrier and InN channel material [4]. The value of the sheet carrier concentrations is larger than that for GaAs-based [5] and GaN-based [6] double heterostructure system.

#### 4.2.2 Composition Dependent Potential Profile and Carrier Concentration

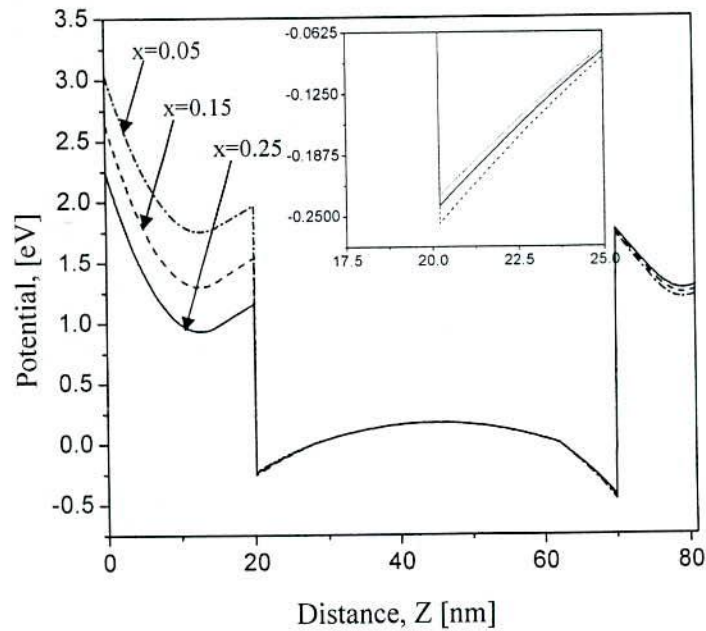


Fig.4.4. Variation of conduction band edge at different mole fraction. Inset: A closer view of  $\text{In}_x\text{Ga}_{1-x}\text{N} / \text{InN}$  region.

The effect of In mole fraction of the upper  $\text{In}_x\text{Ga}_{1-x}\text{N}$  barrier layer on the potential profile is shown in Fig. 4.4. The band offset between  $\text{In}_x\text{Ga}_{1-x}\text{N}$  barrier layer and  $\text{InN}$  channel layer increases with the decrease of In mole fraction of  $\text{In}_x\text{Ga}_{1-x}\text{N}$  because the band gap energy of the  $\text{In}_x\text{Ga}_{1-x}\text{N}$  barrier layer increases with the decrease of mole fraction ( $x$ ) and the conduction band energy discontinuity was assume to be 63% of the band gap difference [4]. The calculated band offset are found to be 2.2 eV, 2.0 eV and 1.8 eV for In content ( $x$ ) of 0.05, 0.15 and 0.25 respectively for  $\text{In}_x\text{Ga}_{1-x}\text{N}$  barrier layer.

The effect of change of In mole fraction ( $x$ ) of the top  $\text{In}_x\text{Ga}_{1-x}\text{N}$  barrier layer on the distribution of carriers in the channel are shown in Fig.4.5. It can be seen that with the increase of In content ( $x$ ), the electron peak concentration decreases. This is due to the weaker carrier confinement with the conduction band offset decreased. Another reason is due to sharp decrease of piezoelectric polarization rather than the slight increase of In content ( $x$ ) in  $\text{In}_x\text{Ga}_{1-x}\text{N}$  barrier layer. From the inset, it is seen that the peak electron concentration is maximum for the In mole fraction  $x=0.05$  and the values of peak electron concentration are found to be  $2.2017 \times 10^{19} \text{ cm}^{-3}$ ,  $1.9715 \times 10^{19} \text{ cm}^{-3}$  and  $1.7705 \times 10^{19} \text{ cm}^{-3}$  for the In content of 0.05, 0.15 and 0.25 respectively. Similar calculations were carried out by Voinigescu et. al. on GaAs-based single and multiple heterojunction HEMTs [7].

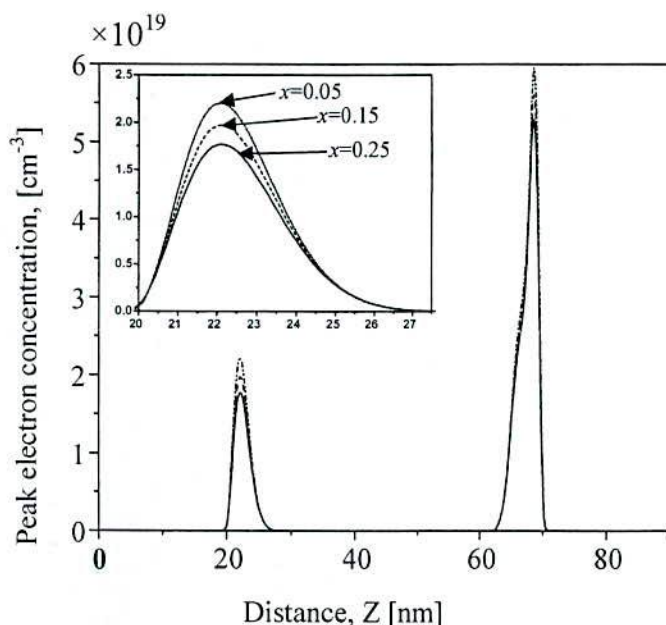


Fig.4.5. Variation of peak electron concentration at different mole fraction. Inset: A closer view of  $\text{In}_x\text{Ga}_{1-x}\text{N} / \text{InN}$  region.



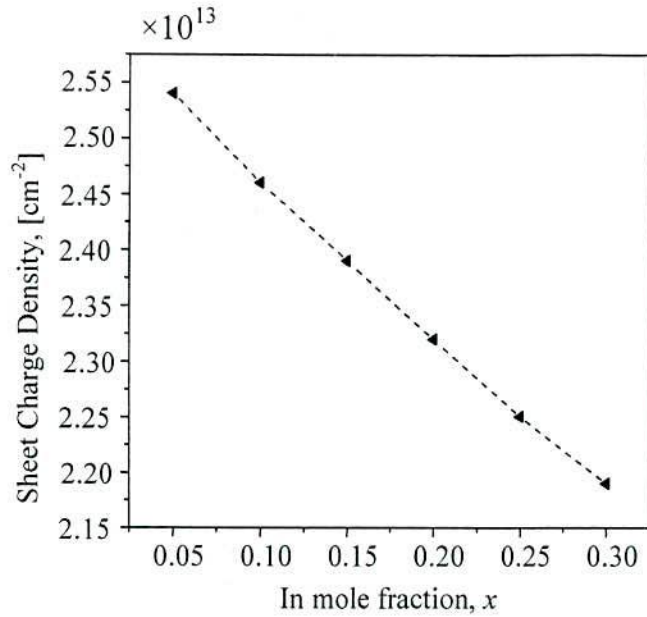


Fig. 4.6 Sheet carrier density versus In mole fraction( $x$ ) of top  $\text{In}_x\text{Ga}_{1-x}\text{N}$  barrier layer.

The variations of sheet charge density for different mole fraction of  $\text{In}_x\text{Ga}_{1-x}\text{N}$  barrier layer is shown in Fig. 4.6. The sheet charge density decreases with the increase of  $x$ . This is due to the decrease of piezoelectric polarization induced charges with small effect of the increase of spontaneous polarization induced charges. The sheet charge density are found to be  $3.69 \times 10^{13} \text{ cm}^{-2}$ ,  $3.54 \times 10^{13} \text{ cm}^{-2}$  and  $3.40 \times 10^{13} \text{ cm}^{-2}$  for In content ( $x$ ) of 0.05, 0.15 and 0.25 respectively. This value of sheet charge density is larger than GaN-based double channel HEMTs [8, 9].

#### 4.2.3 Variation of 2DEG Sheet Carrier Density with Gate to Source Voltage

As the operation principle of DHEMTs is based on the carrier control of 2DEGs by applying an external gate voltage, an accurate carrier control characteristics with gate voltage is very much essential for the characterization and optimization of the proposed device performances. The calculated sheet charge density of electrons in the proposed structure as a function of the gate voltage for different values of In content ( $x$ ) of the  $\text{In}_x\text{Ga}_{1-x}\text{N}$  barrier layer is presented in Fig. 4.7. It is seen that from figure, for a particular gate voltage the sheet carrier increases with the increase in gate voltage from threshold voltage. This variation of sheet carrier concentration is due to increase in conduction band discontinuity ( $\Delta E_c$ ) of the upper heterointerface with the gate voltage. At a gate bias of 0.1 V, the sheet charge density is found to be  $3.69 \times 10^{13} \text{ cm}^{-2}$ ,  $3.54 \times 10^{13} \text{ cm}^{-2}$  and  $3.40 \times 10^{13} \text{ cm}^{-2}$  for In content of 0.05, 0.15 and 0.25 respectively. For a

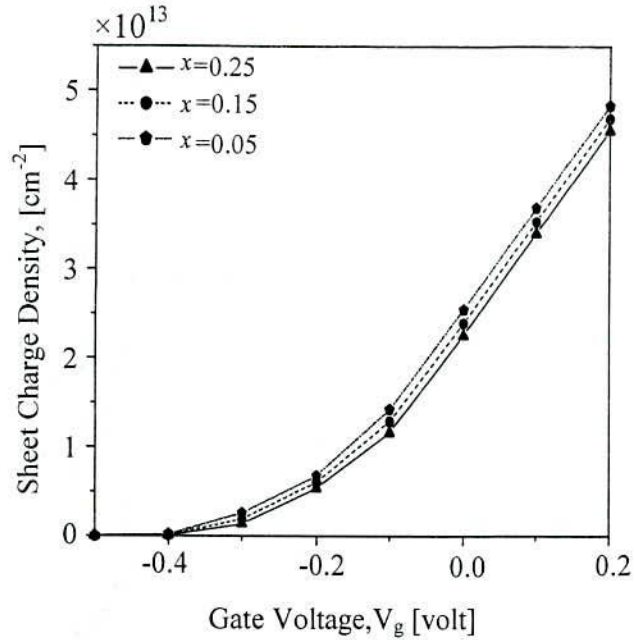


Fig. 4.7 Gate voltage dependence sheet charge density with different In content( $x$ ) for the proposed DHEMT.

particular mole fraction, the slope of the curve corresponds to the capacitance of the structure, which is directly related to the separation between the gate and the 2DEGs, i.e., the thickness of InGaN barrier layer and well width. These parameters are also found by the calculation of the average distance of the 2DEG from the top heterointerface in the section 4.2.5. As the InGaN layer thickness increases, the slope of the curve beyond threshold decreases. Thus, a higher value of InGaN layer thickness is desirable to achieve high value of 2DEG density and lower values of gate capacitance [10]. However, the parallel conduction in dopant layer imposes an upper limit of InGaN layer thickness.

#### 4.2.4 Variation of 2DEG Sheet Carrier Density with Doping of Barrier Layer

Doping is a very important parameter for introducing the carriers in the channel of the heterostructure devices. In Figure 4.8, the calculated results for the dependence of sheet charge density with donor concentration in  $\text{In}_x\text{Ga}_{1-x}\text{N}$  barrier layer for different In mole fraction  $x=0.05$ , 0.15 and 0.25 are plotted. It is observed that the electron sheet concentration increases when the doping density has increased. The calculations also show that the contribution of additional donor impurities on the electron sheet concentration is less effective as the In mole fraction has increased.

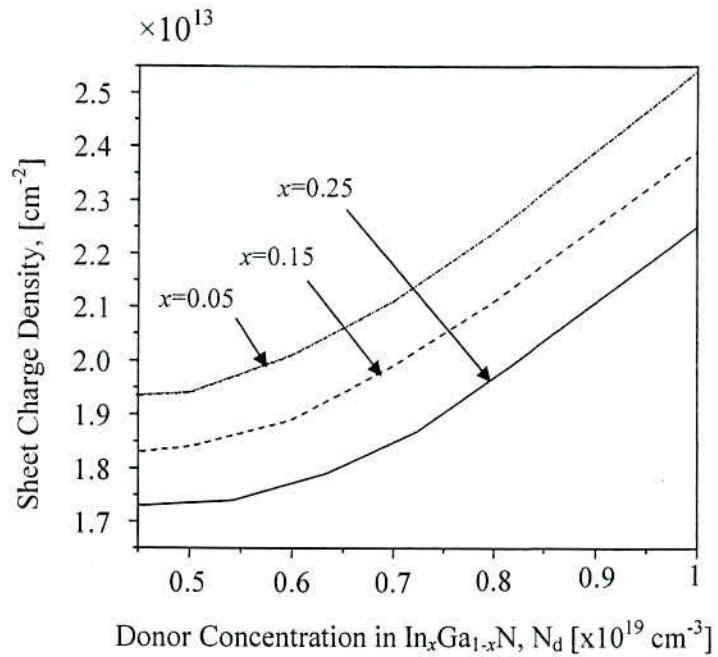


Fig. 4.8 The variation of sheet charge density with donor concentration of top  $\text{In}_x\text{Ga}_{1-x}\text{N}$  barrier layer.

#### 4.2.5 Average Distance of 2DEGs from Top Heterointerface

The average distance of the 2DEGs inside the quantum well from the top heterointerface is shown in Fig. 4.9. Average distance from the top interface (during the inverted HEMT mode) remains approximately constant, while average distance decreases at much faster rate when both channels start to conduct. The results of two channel HEMT contradicts with the single channel structures, where the average distance decreases rapidly [11] with the increase of sheet charge density with the gate bias. During the inverted HEMT mode, the average distance is found to be 44 nm. This average distance starts to decrease with the beginning of normal mode operation of HEMT. The smaller average distance is required for larger gate capacitance, and wider wells give poor gate capacitance; however, a greater two-dimensional spread of electron gas inside the quantum well enhances the carrier mobility. Thus, one must use the optimal well width for high speed operation of the DHEMT devices [5, 12].

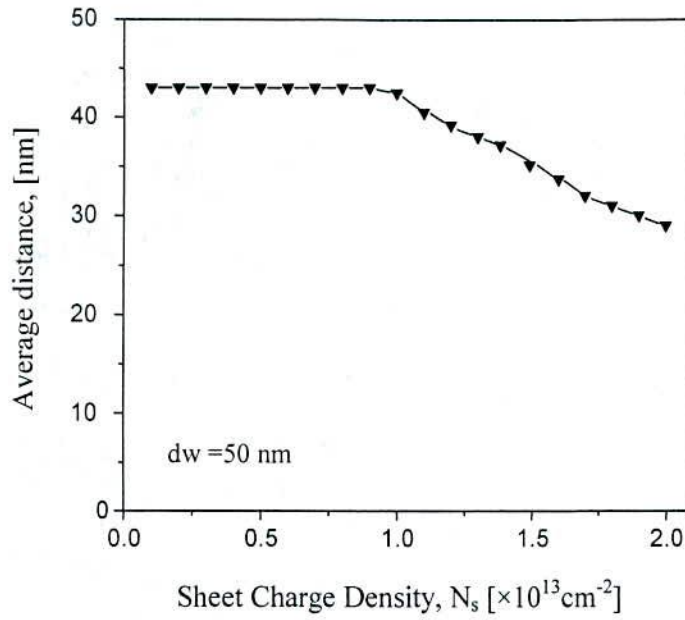


Fig.4.9 Average distance of the 2DEGs from the top heterointerface for the proposed 50 nm well width InN-based DHEMT.

### 4.3 Mobility Analysis

#### 4.3.1 Scattering Mechanisms in InN-Based DHEMTs

When electrons propagate through the semiconductor, they suffer different kinds of scattering. Due to scattering the electrons are slowed down. If one considers a beam of electrons moving initially with the same momentum, then due to the scattering processes, the momentum and energy will gradually lose coherence with the initial state values. The average time takes to loss coherence of the initial state properties is called the relaxation time or scattering time. The total scattering time,  $\tau_{sc}$  can be calculated as a sum of the scattering times due to each scattering process by Matthiessen's rule

$$\frac{1}{\tau_{sc}} = \sum_i \frac{1}{\tau_{sc}^{(i)}} \quad (4.1)$$

Where,  $\tau_{sc}^{(i)}$  is the scattering time of the electrons due to the individual scattering process. The scattering mechanisms have a large effect in limiting the 2DEGs mobility in InN-based DHEMTs. Since the electrons in the interface of heterojunction form two-dimensional states, Monte Carlo simulation requires the use of the scattering rate. The scattering mechanisms considered are dislocations scattering due to the large lattice mismatch, impurity scattering by

remote donors and due to interface charge, interface roughness in InGaN/InN heterointerfaces, alloy disorder scattering due to penetration of the 2DEG wave function into the barrier, and phonons scattering. The detailed analysis for the calculation of mobility with different scattering mechanism is presented in our previously published paper [13].

#### 4.3.1.1 Dislocation Scattering

Due to the large lattice mismatch of InGaN with the substrates on which it is epitaxially grown (SiC and Sapphire), dislocations ( $N_{\text{dis}} = 10^8$  to  $10^{10}$   $\text{cm}^{-2}$ ) are typically formed. These dislocations originate from the nucleation layer at the interface of the substrate and InGaN, growing up to the surface without termination. The dislocations are observed to grow along the (0001) direction, piercing through interfaces.

The model used for the electrical nature of dislocations to study its effect on transport is that of a charged line, the dislocation is modeled as a line of dangling bonds, which introduce states in the energy gap. The dangling bonds are separated by a lattice constant  $c_0$  along the (0001) direction. The line charge density is given by

$$\rho_L = \frac{ef}{c_0} \quad (4.2)$$

where  $e$  is the electron charge and  $f$  (assumed 1) is the fraction of occupied acceptor states introduced by the dislocation [16]. The Fourier transform of the screened potential experienced by the 2DEG due to a differential charge element  $dQ = \rho_L dz$  located a distance  $z$  away from the interface is given by [3]

$$dU(q) = \frac{e\rho_L}{2\varepsilon} \frac{P_0 e^{-qz} dz}{q + q_{TF} G(q)} \quad (4.3)$$

$P_0$  and  $G(q)$  are form factor,  $q_{TF}$  is the Thomas-Fermi screening wave vector for 2D systems, given by  $q_{TF} = 2/a_B^*$ ,  $a_B^*$  being the effective Bohr radius in 2D. The total potential seen at the 2DEG is obtained by summing potentials of all differential elements

$$A(q) = \frac{e\rho_L}{2\varepsilon} \frac{P_0}{q + q_{TF} G(q)} \quad (4.4)$$

The scattering rate is evaluated by using the following equation as

$$\frac{1}{\tau_{dis}} = N_{dis} \left( \frac{m^*}{2\pi\hbar^3 k_F^3} \right)^{2k_F} \int_0^{2k_F} |A(q)|^2 \frac{q^2 dq}{\sqrt{1 - \left( \frac{q}{2k_F} \right)^2}} \quad (4.5)$$

Where,  $k_F = \sqrt{2\pi n_s}$  is the Fermi wave vector, which depends on the 2DEG carrier concentration ( $n_s$ ). Using the screened potential with the substitution  $u = q/2k_F$  we get the scattering rate as [3]

$$\frac{1}{\tau_{dis}} = \frac{N_{dis} m^* e^2 \rho_L^2}{\hbar^3 \epsilon_0^2 \epsilon_b^2} \left( \frac{1}{16\pi k_F^4} \right) \int_0^1 \frac{du}{\left( u + \frac{q_{TF}}{2k_F} \right)^2 \sqrt{1 - u^2}} \quad (4.6)$$

$$= \frac{N_{dis} m^* e^2 \rho_L^2}{\hbar^3 \epsilon_0^2 \epsilon_b^2} \frac{I\left(\frac{q_{TF}}{2k_F}\right)}{16\pi k_F^4} \quad (4.7)$$

The dimensionless integral  $I(q_{TF}/2k_F)$  can be evaluated exactly. It depends only on the 2DEG carrier concentration through the Fermi wave vector, and has an approximate  $\sqrt{n_s}$  dependence. It should be noted that the dislocations affect a transport in the two-dimensional electron gas not only through the Coulomb interaction of electrons with charged dislocation cores, but also due to the induced lattice strain surrounding dislocations [18]. Thus, even if dislocations are uncharged, electrons are scattered by a deformation potential originating from lattice strain in the vicinity to dislocations.

#### 4.3.1.2 Ionized Impurity Scattering

Impurity scatterings for 2DEG carriers can be investigated in two parts; an ionized impurity scattering due to remote donors or surface donors which is effective in modulation-doped structures and an ionized impurity scattering due to interface charges or simply background impurity scattering which is effective in all structures. At low temperature the mobility is dominated by this scattering mechanism.

##### i. Background Impurity Scattering

The spirit of the HEMT 2DEG is a spatial separation of the 2DEG from the ionized donors, thus reducing scattering and improving electron mobility. State of the art InGaN/InN systems have

( $N_{back} = 10^{16}$  to  $10^{18}$  cm $^{-3}$ ) unintentional residual background donors. Transport scattering rate due to a homogeneous background donor density of  $N_{back}$  is given by

$$\frac{1}{\tau_{back}} = N_{back} \frac{m^*}{2\pi\hbar^3 k_F^3} \left(\frac{e^2}{2\epsilon}\right)^{2k_F} \int_0^{2k_F} dq \frac{P_0^2}{(q + q_{TF} G(q))^2} \frac{q}{\sqrt{1 - \left(\frac{q}{2k_F}\right)^2}} \quad (4.8)$$

The absence of intentional modulation donors implies that there is a different source of 2DEG electrons. The polarization by itself cannot supply electrons, since on the whole, it is charge neutral. Background impurity densities cannot be the source of the 2DEG electrons since their concentration is too low for providing the high density 2DEG densities observed.

### ii. Surface Donor Scattering

Electrons in the 2DEG for nitride heterostructures are believed to be supplied by surface donor states. The positive surface charge forms a sheet-charge dipole with the 2DEG which tries to neutralize the polarization dipole in the InGaN layer. These experiments confirm the suspicion that the surface states are charged, and are responsible for forming the 2DEGs, as inferred from a purely charge control analysis by Ibbotson [19].

The surface donor states will form a source of scattering identical to a delta-doped remote donor layer. Thus, the transport scattering rate for the surface donors can be treated in the same way as an ordinary delta-doped donor layer. If the sheet density of such donors is  $N_s$  ( $10^{13}$  cm $^{-2}$ ), and is at a distance  $d$ , from the heterostructure interface (note that this is also the thickness of the InGaN barrier), the scattering rate is given by

$$\frac{1}{\tau_r} = N_s \frac{m^*}{2\pi\hbar^3 k_F^3} \left(\frac{e^2}{2\epsilon}\right)^{2k_F} \int_0^{2k_F} dq \frac{P_0^2 e^{-2q|d|}}{(q + q_{TF} G(q))^2} \frac{q^2}{\sqrt{1 - \left(\frac{q}{2k_F}\right)^2}} \quad (4.9)$$

#### 4.3.1.3 Alloy Disorder Scattering

Alloy disorder scattering originates from the randomly varying alloy potential in the barrier. Although the centroid of the 2DEG is in the binary material InN, there is a penetration of the wavefunction into the ternary InGaN barrier. As expected, the lower the In mole fraction, the lower the probability of the penetration because the discontinuity between the conduction band of InN and that of lower In mole fraction InGaN, i.e. effective barrier height, is larger. It is also

noted that the penetration becomes larger when the carrier density increases. The shift of the wavefunction towards to the interface can partially explain the decrease of the mobility when the sheet charge density increases. The deeper penetration implies more alloy disorder scattering. As the wavefunction moves closer to the interface of the 2DEG the interface roughness scattering becomes more obvious. Scattering rate by alloy disorder is given by [20]

$$\frac{1}{\tau_{alloy}} = \frac{3b}{16} \frac{x(1-x)m^*\Omega_0 U_{AL}^2}{\hbar^3} \quad (4.10)$$

where  $x$  is the alloy mole fraction,  $\Omega_0$  is the volume occupied by one atom and  $U_{AL}$  is the alloy potential. The factor  $b$  is called the Fang–Howard expression [21] of wavefunctions for Hartree approximation of a triangular well and is given by [22]

$$b = \left( \frac{33e^2 m^* n_{2D}}{8\epsilon_0 \epsilon_s \hbar^2} \right)^{\frac{1}{3}} \quad (4.11)$$

#### 4.3.1.4 Interface Roughness Scattering

Interface roughness is an important problem for semiconductor heterostructures [23]. It can lead to the perturbation of electron energy [24]. Narrow quantum wells of InGaN/InN heterostructures are more sensitive to interface roughness that can lead to a large fluctuation in the quantized electron energies [25]. Scattering at rough interfaces can be severed if the 2DEG density is high, since the 2DEG tends to shift closer to the interface as the density increases. Scattering rate by a rough interface with a root mean square roughness height,  $\Delta$  and a correlation length between fluctuations,  $L$  is given by [26]

$$\frac{1}{\tau_{ir}} = \frac{\Delta^2 L^2 e^4 m^*}{2\epsilon^2 \hbar^3} \left( \frac{1}{2} n_{2D} \right)^2 \int_0^1 du \frac{u^4 e^{-k_F^2 L^2 u^2}}{\left( u + G(u) \frac{q_{TF}}{2k_F} \right)^2 \sqrt{1-u^2}} \quad (4.12)$$

where, the integral is rendered dimensionless by the substitution  $u = q/2k_F$ .

Interface roughness scattering affects transport even in the presence of a binary barrier (i.e., absence of alloy scattering). In such high-density samples, the mobility is interface roughness scattering limited, and the calculated low temperature mobilities are well explained by the theory. Interface roughness scattering limited transport mobility has a characteristic  $L^{-6}$  dependence for 2DEGs in quantum wells (of thickness  $L$ ), which can be observed by transport measurements on quantum wells of different thicknesses. An interesting feature of the III-



nitrides is that due to the unscreened polarization fields in thin epitaxial layers, there is a large band-bending inside the well even under no external bias. Hence the 2DEG samples one interface much more than the other; this acts as an in-built mechanism to restrict interface roughness effects on 2DEGs confined in thin unscreened quantum wells.

#### 4.3.1.5 Phonon Scattering

Phonon scattering plays an important role in limiting the electron mobility in III–nitride semiconductors. The three most important phonon-scattering processes are deformation potential acoustic, piezoelectric acoustic, and polar optical.

##### i. Acoustics Phonon Scattering

At intermediate temperatures, the acoustic phonon scattering is another important scattering mechanism. In this work, we use the elastic acoustic phonon scattering model proposed by Ridley et al [27]. The acoustic phonon scattering is calculated by considering two scattering mechanisms, including deformation potential and piezoelectric scattering. The expression of deformation potential scattering is given by [27]

$$\frac{1}{\tau_{dp}} = \frac{3b}{16} \frac{\Xi^2 k_B m^* T}{\hbar^3 \rho u_l^2} I_{DP}(k) \quad (4.13)$$

Here,  $\rho$  is the crystal density,  $u_l$  is the longitudinal acoustic phonon velocity and  $\Xi$  is the deformation potential.

In equation,  $I_{DP}(k)$  is the integral

$$I_{DP}(k) = \int_0^{2k} \frac{1}{2\pi k^3 (q + q_s)^2 \sqrt{1 - \left(\frac{q}{2k}\right)^2}} q^4 dq \quad (4.14)$$

In this integral,  $q_s$  is the two-dimensional reciprocal length which is defined as

$$q_s = \frac{e^2 m^*}{2\pi \hbar^2 \epsilon_0 \epsilon_s} F_{11}(q) f(0) \quad (4.15)$$

where  $f(0)$  is the occupation probability at the subband which can be assumed that all screening is determined the lowest subband electrons [27].  $F_{11}(q)$  is the form factor the ground-state Fang–Howard wavefunction [21]. In strongly polar materials such as InN the acoustic are strongly interacted by the piezoelectric effect. The form factor  $F(q)$  is given by [28]

$$F(q) = \int_0^{\infty} dz \int_0^{\infty} dz' [f(z)]^2 [f(z')]^2 e^{-q|z-z'|} \quad (4.16)$$

Mobility expression of piezoelectric scattering with a of angular dependence is given by [27]

$$\frac{1}{\tau_{pe}} = \frac{e^2 K^2 k_B m^* T}{\pi \epsilon_0 \epsilon_s \hbar^3 k} I_{PE}(k) \quad (4.17)$$

In the above equation,  $K$  is the electromechanical coupling coefficient and given by [29]

$$K^2 = \frac{\epsilon_{LA}^2}{\epsilon_s c_{LA}} - \frac{\epsilon_{TA}^2}{\epsilon_s c_{TA}} \quad (4.18)$$

In the above equation,  $\epsilon_{LA}$ ,  $\epsilon_{TA}$ ,  $c_{LA}$ ,  $c_{TA}$  are the effective piezoelectric constants and the averaged elastic constants related to longitudinal and transverse acoustic phonons, respectively. The integral  $I_{PE}(k)$  is in the form

$$I_{PE}(k) = \int_0^{2k} \frac{F_{11}(q)}{4k^2 (q + q_s)^2 \sqrt{1 - (\frac{q}{2k})^2}} q^3 dq \quad (4.19)$$

It is interesting to note that the acoustic phonon scattering has a negligible effect on the 2DEG mobility. However, the acoustic phonon scattering mechanism is, in general, found as a main scattering mechanism at intermediate temperature [30–32].

## ii. Optical Phonon Scattering

At high temperatures, the mobility of a 2D carrier is mostly limited by polar optic phonon scattering. The expression of the mobility limited by the polar optic phonon scattering is given by Ridley as [17]

$$\frac{1}{\tau_{po}} = \frac{e^2 \omega m^* Z_0}{4\pi \epsilon_0 \epsilon_p \hbar^2} \left[ \frac{1}{e^{\hbar\omega/k_B T} - 1} \right] \quad (4.20)$$

$$\text{where, } \frac{1}{\epsilon_p} = \frac{1}{\epsilon_\infty} - \frac{1}{\epsilon_0}$$

Here,  $\hbar\omega$  is the polar optic phonon energy,  $m^*$  is the effective mass for electron;  $\epsilon$  and  $\epsilon_s$  are the high and low frequency dielectric constants, respectively. There large effect large effects on optical phonon scattering.

### 4.3.2 Overall Mobility

The 2DEGs Mobility is calculated by

$$\mu = \frac{e \langle \tau_{tot} \rangle}{m_e^*} \quad (4.21)$$

where,  $\mu$  = Mobility,  $\langle \tau_{tot} \rangle$  = Mean scattering time calculated using Monte Carlo Simulation,  $e$  = Electron charge,  $m_e^*$  = Electron effective mass.

The simulation starts with one electron with wave vector; then the duration of the first free flight is chosen with a probability distribution determined by the scattering probabilities. A new state after scattering is randomly chosen as initial state of the new free flight and entire processes is iteratively repeated. Reliable results are usually obtained within 80-100 thousands scattering events. The mean value relaxation time can be calculated by taking an average over all free flights. Then from this mean relaxation time the mobility of the material can be easily obtained. During simulation, the electron population in the device adjusts itself so that the overall charge neutrality is satisfied.

A low temperature mobility map as a function of the 2DEG sheet carrier ( $n_s$ ) is shown in Fig. 4.10. All probable sources of scattering have been considered, and the relative effects are clearly shown in the Fig. 4.10. Total mobility shows a characteristic maximum at low sheet densities ( $n_s \leq 5 \times 10^{12} \text{ cm}^{-2}$ ) for a low temperature ( $T < 80 \text{ K}$ ).

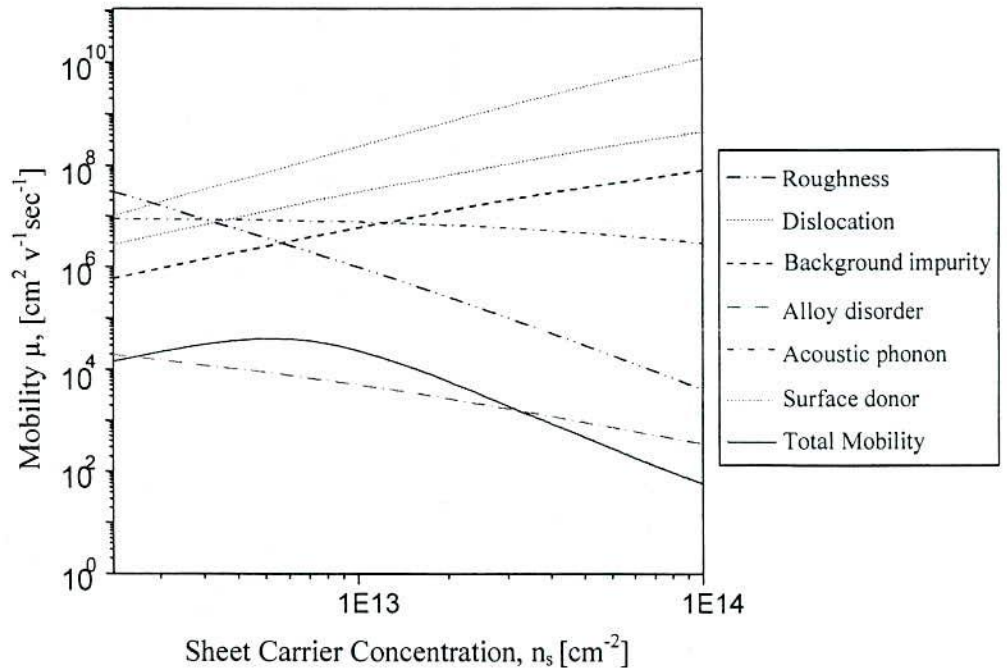


Fig. 4.10. Scattering processes limiting the 2DEGs mobility in InGaN/InN/InGaN heterostructures at 77K.

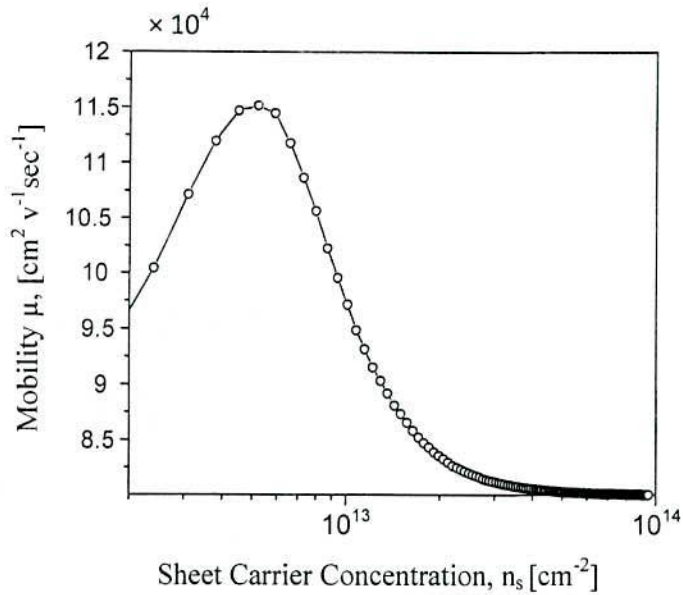


Fig. 4.11 Total mobility of the 2DEGs in the proposed InN based DHEMT structures at 77K.

At low temperature the dislocation, background impurity, and surface donor scattering mechanisms are found to be dominated for a lower values of sheet carrier. While alloy disorder and interface roughness is found to be dominated over the entire sheet carrier range, depending on the nature of the InGaN barrier. At 77 K the maximum total 2DEGs mobility is found to be  $11.5 \times 10^4 \text{ cm}^2 \text{V}^{-1} \text{s}^{-1}$  at a sheet carrier concentration,  $n_s = 5.2 \times 10^{12} \text{ cm}^{-2}$  which is clearly shown in Fig. 4.11. These results are comparable to GaAs and GaN- based Double Heterostructure system [14, 15].

#### 4.4 Velocity Field Characteristics

In most electronic devices a significant portion of the electronic transport occurs under strong electric fields. This is especially true for DHEMTs. At such high fields ( $E \sim 1\text{-}100 \text{ kVcm}^{-1}$ ) the electrons get “hot” and acquire a high average energy. The extra energy comes due to the strong electric fields. The drift velocities are also quite high. The description of electrons at such high electric fields is quite complex and requires either numerical techniques or computer simulations. At high electric field as the carriers gain energy from the field, they suffer greater rates of scattering. The mobility thus starts to decrease. It is usual to represent the response of the carriers to the electric field by velocity-field relations. At very high fields the drift velocity becomes saturated, i.e., becomes independent of the electric field. The drift velocity for carriers

in most materials saturates to a value of  $\sim 10^7$   $\text{cm/s}$ . The fact that the velocity saturates is very important in understanding current flow in semiconductor devices.

The calculations are carried out using Monte Carlo simulation and the calculated result is shown in Fig. 4.12. At room temperature the peak velocity for DHEMTs is found to be  $4.95 \times 10^7$   $\text{cm/sec}$  at the field  $57.5$   $\text{kV/cm}$  which is less than for single channel HEMTs [5]. The velocity reduction for higher electron mobility at smaller electric fields can be attributed to the result of the appearance of polar optical emissions as the electrons are rapidly heated due to the higher mobility. Furthermore, the inter-subband scattering also increases due to the reduction of the intersubband gap with the increases of sheet charge density. Consequently, the electrons are further heated up and then the intervally transition from the centre to the satellite valley can be enhanced [5]. Therefore higher carrier density brings the lower velocity in a high field. The velocity characteristics for the DHEMTs show a higher value in a low field and a lower value in a high field. This feature is suitable for DHEMTs operation because it has a high carrier density channel in the source region and relatively low carrier density channel in the drain region. So, the high carrier density channel and high electron mobility can reduce the parasitic resistance, and then the velocity-field characteristics in double heterostructure are appropriate to DHEMTs device operation.

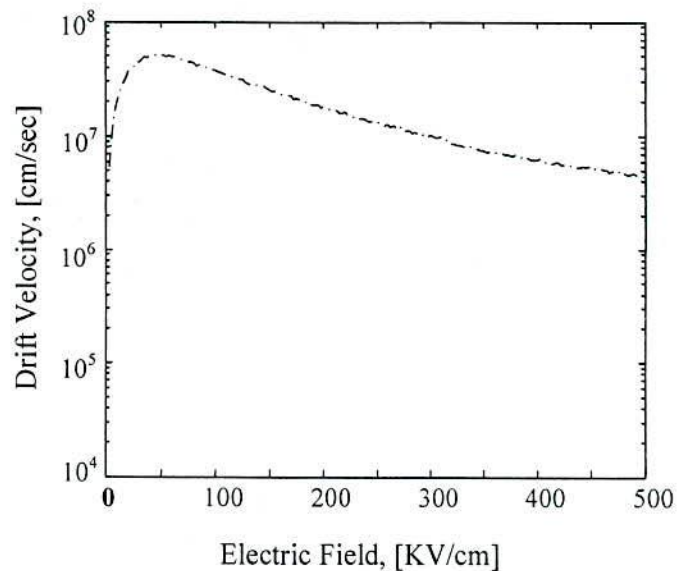


Fig: 4.12 Velocity-field characteristics of the proposed InGaN/InN/InGaN based DHEMT.

## References

- [1] B. Vinter, "Subbands and charge control in a two-dimensional electron gas field-effect transistor," *Appl. Phys. Letter*, vol. 44, pp. 307, (1984).
- [2] A. Rashmi, A. Kranti, S. Haldar, R. S. Gupta, "An accurate charge control model for spontaneous and piezoelectric polarization dependent two-dimensional electron gas sheet charge density of lattice-mismatched AlGaIn/GaN HEMTs," *Solid-State Electronics*, vol. 46, pp. 621–630, (2002).
- [3] T. Ando, A. B. Fowler, and F. Stern "Electronic properties of two-dimensional systems," *Review on Modern Physics*, vol. 54, pp. 437-672, (1982).
- [4] M. T. Hasan, A. G. Bhuiyan, and Akio Yamamoto, "Two dimensional electron gas in InN-based heterostructures: Effects of spontaneous and piezoelectric polarization," *Solid-State Electronics*, vol. 52, pp. 134, (2008).
- [5] M. Tomizawa, T. Furuta, K. Yokoyama, "Modeling of electron transport in AlGaAs/GaAs/AlGaAs Double Heterojunction Structure," *IEEE Trans. on ED*, vol. 36, no. 11, pp. 2380-2385, (1989).
- [6] C. Q. Chen, J. P. Zhang, V. Adivarahan, A. Koudymov, H. Fatima, G. Simin, J. Yang, and M. A. Khan, "AlGaIn/GaN/AlGaIn double heterostructure for high-power III-Nitride field-effect transistors," *Applied Physics Letter*, vol. 82, no. 25, 23 June, (2003).
- [7] Sorin Voinigescu, "Quantum Modelling of charge distribution in single and multiple heterojunction MODFETs," *Int. J. Electronics*, vol. 66, no. 2, pp. 227-245, (1989).
- [8] R. Chu, Y. Zhou, J. Liu, "AlGaIn-GaN double-channel HEMTs," *IEEE Trans. on Electron Devices*, vol. 52, pp. 438, (2005).
- [9] R. Gaska, M. S. Shur, T. A. Fjeldly, "Two-channel AlGaIn/GaN heterostructure field effect transistor for high power applications," *J. Appl. Phys.*, vol. 85, pp. 3009, (1999).
- [10] R. Aggarwal, A. Agrawal, M. Gupta and R. S. Gupta, "Analytical performance evaluation of AlGaIn/GaN metal insulator semiconductor heterostructure field effect transistor and its comparison with conventional HFETs for high power microwave applications," *Microwave and optical technology letters*, vol. 50, no. 2, February (2008).

- [11] A. Shey and H. K. Walter, "On the Charge Control of the two dimensional Electron Gas for Analytic Modeling of HEMT's," IEEE Electron Device Letter, vol. ED-9, no. 12, pp. 624-626, (1988).
- [12] J. M. Lagemaat, G. E. W. Bauer, J. J. Harris and C. T. Foxon, "Coupling of electron gases in wide quantum wells," Physical Review (B), vol. 38, no. 18, Dec. (1988).
- [13] M. T. Hassan, M. R. Kaysir, M. S. Islam, M. R. Islam and A. G. Bhuiyan, A. Yamamoto, "2DEG properties in InGaN/InN/InGaN-based double channel HEMTs," Physica Status Solidi (c), vol. 7, no. 7-8, pp. 1997-2000, (2010).
- [14] K. Inoue and H. Sakaki, "A New Highly Conductive (AlGa)As/GaAs/(AlGa)As Selectively-doped Double Heterojunction Field Effect Transistor," Jap. Jour. of App. Physics, vol. 23, no. 2, pp- L61-L63, (1984).
- [15] N. Maeda, T. Saitoh, K. Tsubaki, T. Nishidi, "Two-Dimensional Electron Gas Transport Properties in AlGaN/(In)GaN/AlGaN Double-Heterojunction Field Effect Transistors," Journal of Applied Physics., vol. 30, pp. 729, (2003).
- [16] D. Jena, A. C. Gossard, and U. K. Mishra, "Dislocation scattering in a two-dimensional electron gas," Appl. Phys. Lett., vol. 76, no. 13, pp. 1707-1709, (2000).
- [17] K. Lee, M. S. Shur, T. J. Drumond and H. Morkoc, "Current-Voltage and capacitance-Voltage characteristics of modulation-doped field-effect transistors," IEEE Trans. Electron Devices, vol. 30, pp. 207, (1983).
- [18] Debdeep Jena and U. K. Mishra, "Effect of scattering by strain fields surrounding edge dislocations on electron transport in two-dimensional electron gases", Appl. Phys. Lett., vol. 80, no. 1, pp. 64-66, (2002).
- [19] J. P. Ibbetson, P. T. Fini, K. D. Ness, S. P. Den Baars, J. S. Speck, and U. K. Mishra "Polarization effects, surface states, and the source of electrons in AlGaIn/GaN heterostructure field effect transistors," Appl. Phys. Lett., vol. 77, pp. 250, (2000).
- [20] M. J. Kearney and A. I. Horrell, "The effect of alloy scattering on the mobility of holes in a  $\text{Si}_{1-x}\text{Ge}_x$  quantum well," Semicond. Sci. Technol., vol. 13, pp. 174, (1998).
- [21] F. F. Fang and W. E. Howard, "Negative Field-Effect Mobility on (100) Si Surfaces," Phys. Rev. Lett., vol. 16, pp. 797, (1966).

- [22] J. H. Davies, "The Physics of Low-Dimensional Semiconductors," Cambridge: Cambridge University Press, (1998).
- [23] D. Zanato, S. Gokden, N. Balkan, B. K. Ridley and W. J. Schaff, "The effect of interface-roughness and dislocation scattering on low temperature mobility of 2D electron gas in GaN/AlGaN," *Semicond. Sci. Technol.*, vol. 19, pp. 427, (2004).
- [24] P. F. Fewster, N. L. Andrew and C. J. Curling, "Interface roughness and period variations in MQW structures determined by X-ray diffraction," *J. Appl. Cryst.*, vol. 21, pp. 524, (1988).
- [25] B. Deveaud, J. Y. Emergy, A. Chomette, B. Lambert and M. Baudet, "Single monolayer well size fluctuations in the luminescence of GaAs-GaAlAs superlattices," *Superlattice and Microstructure*, vol. 3, pp. 205, (1985).
- [26] Debdeep Jena, Yulia Smorchkova, Chris Elsass, Arthur C. Gossard, and Umesh K. Mishra, "Electron transport and intrinsic mobility limits in two-dimensional electron gases of III-V nitride heterostructures," *arxiv: cond-mat*, vol. 1, no. 0103461, (2001).
- [27] B. K. Ridley, B. E. Foutz and L. F. Eastman, "Mobility of electrons in bulk GaN and  $\text{Al}_x\text{Ga}_{1-x}\text{N}/\text{GaN}$  heterostructures," *Phys. Rev. B*, vol. 61, pp. 16862 (2000).
- [28] K. Hirakawa and H. Sakaki, "Mobility of the two-dimensional electron gas at selectively doped n-type  $\text{Al}_x\text{Ga}_{1-x}\text{As}/\text{GaAs}$  heterojunctions with controlled electron concentrations," *Phys. Rev. B*, vol. 33, pp. 8291-8303, (1986).
- [29] M. Ramonas, A. Matulionis and L. Rota, "Monte Carlo simulation of hot-phonon and degeneracy effects in the AlGaIn/GaN two-dimensional electron gas channel" *Semicond. Sci. Technol.*, vol. 18, pp. 118, (2003).
- [30] S. Gokden, A. Ilgaz, N. Balkan and S. Mazzucato, *Physica E*, Vol. 25, pp. 86 (2004).
- [31] R. Gaska, J. W. Yang, A. Osinsky, Q. Chen, M. A. Khan, A. O. Orlov, G. L. Snider and M. S. Shur, "Electron transport in AlGaIn-GaN heterostructures grown on 6H-SiC substrates," *Appl. Phys. Lett.*, vol. 72, pp. 707, (1998).
- [32] D. Huang, F. Yun, M. A. Reshchikov, D. Wang, H. Morkec, D. L. Rode, L.A. Farina, C. Kurdak, K. T. Tsen, S. S. Park, K. Y. Lee, "Hall mobility and carrier concentration in free-standing high quality GaN templates grown by hybrid vapor phase epitaxy," *Solid State Electron.*, vol. 45, pp. 711, (2001).



## Chapter V

### Performance of DHEMTs

#### 5.1 Introduction

To realize the performance of the proposed InN-based DHEMTs, this chapter focuses the dc characteristics i.e. current-voltage and transconductance of the DHEMTs. The current-voltage characteristic is determined from the self consistent quasi-one dimensional calculations as discussed in the chapter-III. The transconductance is calculated for the proposed DHEMT. The characteristic of these output performances are also discussed.

#### 5.2 Current-Voltage Characteristics

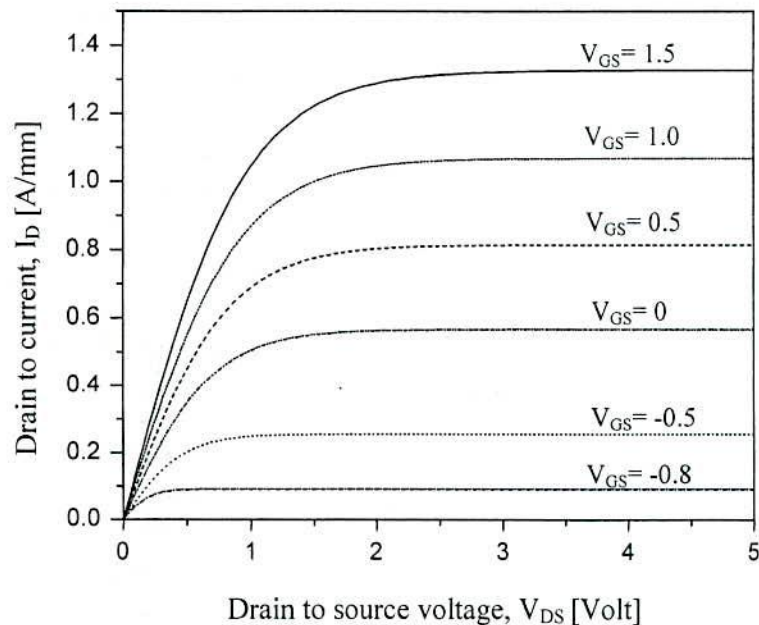


Fig. 5.1 DC current-voltage characteristics of the the proposed InN-based double channel HEMT for 0.1  $\mu\text{m}$  gate length.

The calculated current voltage characteristics for several gate biases for 0.1  $\mu\text{m}$  gate length DHEMT device are shown in Fig. 5.1.  $I_D$  increases linearly with the increase in  $V_{DS}$  in the low longitudinal field region (linear region) up to pinch off. After this value,  $I_D$  doesn't vary

significantly. Drain current also increases with the increase in  $V_{GS}$  because with increase in gate to source voltage the sheet carrier concentration increases. Maximum drain current is found to be 1.325 A/mm for proposed DHEMT at  $V_{GS}=1.5V$  for different values of drain source voltage. The channel current is larger than conventional InN-based HFETs [1]. The major cause for this rise is due to the increase in channel carrier density by double heterostructure system. A similar increase in maximum drain saturation current was also reported in GaN-based double heterostructure HEMT by Chen et al. [2].

### 5.3 Transfer Characteristics

The variation of drain current with gate bias for  $0.1\mu\text{m}$  gate length InGaN/InN/InGaN DHEMTs is depicted in Fig. 5.2. At the gate to source voltage ( $V_{GS}$ ) is increased from the threshold voltage, the depth of the potential well at the upper heterointerface increases, resulting the higher sheet carrier concentration and higher drain current. The dc saturation drain current, which is a key parameter for controlling maximum output RF power, is larger in DHEMTs than in HEMTs [3]. The forward gate current, which increases exponentially as a function of gate

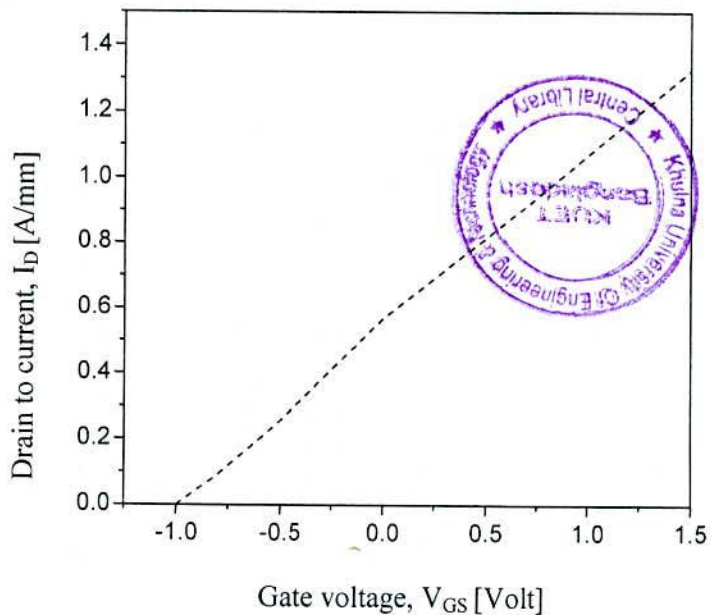


Fig. 5.2 Transfer characteristics of the proposed InN-based double channel HEMT with  $V_{DS} = 4$  V.

bias, plays significant role in limiting the channel current at high positive gate biases in DHEMTs. A value of maximum saturation drain current is found to be 1.068 A/mm at  $V_{GS}=1V$  for the proposed DHEMTs. This high value of drain saturation current makes InN-based DHEMT extremely attractive for microwave and millimeter wave applications.

#### 5.4 Transconductance Characteristics:

Figure 5.3 shows the transconductance as a function of the gate voltage. It is seen that transconductance increases with the increase of gate voltage and after reaching the maximum value it starts to decrease. The peak value of  $G_m$  occurs at the  $V_{GS}$  that just cause to form the upper channel and also begin some noticeable occupations of ionized donors under the gate. The peak value of  $G_m$  is found to be 620 mS/mm at  $V_{DS}=4V$ , which is higher than the simulated as well as experimentally obtained value for AlGaIn/GaN double channel HEMTs [4, 5]. This high value of  $G_m$  has been attributed to high saturation velocities and high sheet carrier density. Also this DHEMT device shows less variation of transconductance for wide range of gate to source voltages, which makes it useful for high performance amplifications in microwave and millimeter wave application.

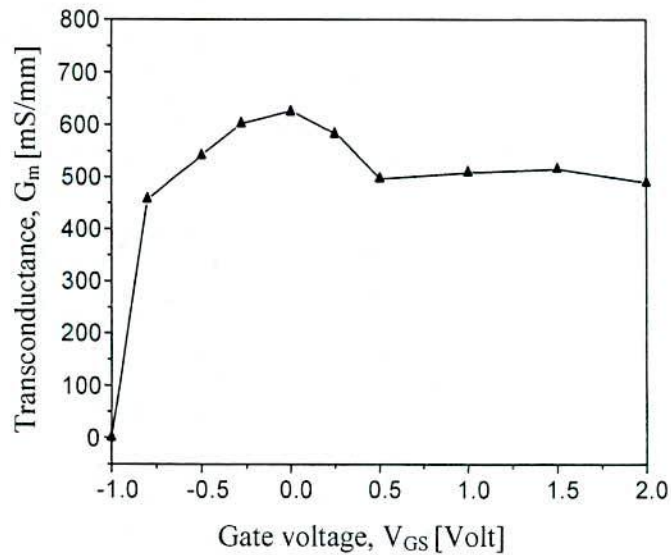


Fig. 5.3 Simulated transconductance ( $G_m$ ) versus  $V_{GS}$  at  $V_{DS} = 4V$  of the the proposed InN-based double channel HEMT.

### References:

- [1] M. S. Islam, S. M. Muhtadi, Md. T. Hasan, A. G. Bhuiyan, Md. R. Islam, A. Hashimoto, and A. Yamamoto, "AlInN/InN metal oxide semiconductor heterostructure field effect transistor," *Phys. Stat. Sol.(C)*, vol.7, no.7/8, pp. 1983–1987, Jul. (2010).
- [2] C. Q. Chen, J. P. Zhang, V. Adivarahan, A. Koudymov, H. Fatima, G. Simin, J. Yang and M. Asif khan, "AlGa<sub>N</sub>/Ga<sub>N</sub>/AlGa<sub>N</sub> double heterostructure for high power III-N field effect transistors," *Applied Physics Lett.*, vol. 82, no. 25, 23 June, (2003).
- [3] A. Vescan, H. Hardtdegen, N. Kettenib, "Study on growth and electrical performance of double-heterostructure AlGa<sub>N</sub>/Ga<sub>N</sub>/AlGa<sub>N</sub> field-effect transistors," *Phys. Stat. Sol. (C)*, vol.6, no.52, pp. 1003–1006, (2009).
- [4] Q. Si, H. Yue, M. Xiaohua, Z. Pengtian and X. Yuanbin, "AlGa<sub>N</sub>/Ga<sub>N</sub> double-channel HEMT," *Journal of Semiconductors*, vol.31, no. 4, April (2010).
- [5] Rongming Chu, Yugang Zhou, Jie Liu, Deliang Wang, Kevin J.Chen, Kei May Lau, "AlGa<sub>N</sub>-Ga<sub>N</sub> Double-Channel HEMTs", *IEEE Transactions on Electron Devices*, vol.52, no.4, April (2005).

## Chapter VI

### Conclusions and Future Work

#### 6.1 Conclusions

Indium Nitride (InN) based semiconductor devices have been intensively investigated over the last few years due to their inherent material properties; high saturation and peak carrier velocity, good thermal conductivity, high dielectric constant and direct bandgap. These physical properties enable InN-based Double Channel High Electron Mobility Transistors (DHEMTs) to be most suitable for high power & high frequency applications. In this dissertation, InN-based DHEMTs have been investigated through theoretical studies, physical modeling and numerical simulations of device operation. A quantum mechanical charge control model of DHEMTs based on InGaN/InN/InGaN double heterostructure using self-consistent solution of 1D Schrödinger-Poisson equations is developed for the characterization and optimization of the device performances. In order to realize the device performance, a comprehensive quasi-2D model based on the solution of 1D Schrodinger-Poisson-drift diffusion equations is developed. Finally, this quasi-2D model is extended to calculate the dc output characteristics i.e. current-voltage characteristics and transconductance so as to predict the microwave performance of the device.

The transport properties provide an ideal platform for the in-depth investigation of InN-based DHEMTs. Among the transport properties electron density and mobility of 2DEGs are two most important concerns. As the operation principle of DHEMTs is based on the carrier control of 2DEGs by applying an external gate voltage, an accurate carrier control characteristics with gate voltage is very much essential. At a gate voltage ( $V_g$ ) of -0.4 V, the bottom channel starts to conduct. The sheet charge density at the bottom channel increases with the increase of gate voltage until the bottom channel becomes saturated and simultaneously the top channel starts to conduct. The 2DEG peak electron concentration for bottom and top channel are found to be  $1.25 \times 10^{20} \text{ cm}^{-3}$  and  $0.89 \times 10^{20} \text{ cm}^{-3}$  respectively at a gate voltage of 0.4 V with In content ( $x$ ) of 0.05 in the  $\text{In}_x\text{Ga}_{1-x}\text{N}$  barrier layer. The composition dependent potential profile and carrier concentration are also investigated for the proposed double heterostructure quantum well system. The peak electron concentrations are found to be  $2.2017 \times 10^{19} \text{ cm}^{-3}$ ,  $1.9715 \times 10^{19} \text{ cm}^{-3}$  and  $1.7705 \times 10^{19} \text{ cm}^{-3}$  for the  $x$  of 0.05, 0.15 and 0.25 respectively at a zero gate voltage. The peak electron concentration decreases with the increase of  $x$  and this is due to decrease of the

band offset between  $\text{In}_x\text{Ga}_{1-x}\text{N}$  barrier layer and InN channel layer. The variation of sheet carrier density with gate voltage is very significant parameter for DHEMT characteristics. By varying the gate voltage -1.0 V to 0.4 V the maximum sheet carrier density found to be  $1.25 \times 10^{14} \text{ cm}^{-2}$ . The value of sheet carrier increases with the increase in  $V_g$  from threshold voltage due to increase in conduction band discontinuity in the upper InGaN barrier layer of DHEMT. This high sheet carrier density is due to the quantum confinement effect caused by the large conduction band offset and the polarization induced sheet charge density owing to the lattice mismatch between  $\text{In}_x\text{Ga}_{1-x}\text{N}$  barrier and InN channel material. The sheet carrier densities obtained are higher than the conventional InN-based HEMT devices [1] and GaN-based double channel HEMTs [2]. The carrier mobility is another very important issue for device performance. The highest mobility for the DHEMT is found to be  $11.5 \times 10^4 \text{ cm}^2\text{V}^{-1}\text{sce}^{-1}$  at  $n_s = 5.2 \times 10^{12} \text{ cm}^{-2}$  at 77 K. The peak velocity of the carrier for the proposed device is found to be  $4.95 \times 10^7 \text{ cmsec}^{-1}$  at the field of 57.5 kV/cm. The drift velocity is smaller than single channel InN based HEMTs [3]. This velocity reduction for higher electron mobility at smaller electric fields can be attributed to the result of the appearance of polar optical emissions as the electrons are rapidly heated due to the higher mobility. The high carrier density channel and high electron mobility can reduce the parasitic resistance, and then the velocity-field characteristics in double heterostructure are appropriate to DHEMTs device operation.

The performance of the InGaN/InN/InGaN DHEMT device includes drain current and transconductance. The maximum drain current density was found to be 1325 mA/mm for the proposed InN-based DHEMT at gate to source voltage ( $V_{GS}$ ) of 1.5 V for different values of drain to source voltage for 0.1  $\mu\text{m}$  gate length. The drain current is found to be higher for the DHEMTs in comparison to GaN-based double channel HEMT [2, 4]. The peak value of transconductance ( $G_m$ ) was found to be 620 mS/mm for DHEMT at  $V_{DS}$  of 4V, which is higher than the reported value for GaN double channel DHFET [2, 5]. High value of  $G_m$  has been attributed to high saturation velocities and high sheet carrier density.

The above achievements indicate the potentiality of InN-based DHEMT for future high performance high speed microwave and millimeter wave devices and more attention should be given on it.

## 6.2 Future Work

This dissertation presented a detailed study about the theoretical one dimensional numerical modeling and performance evolution of InN-based DHEMT for high speed and high frequency applications. There are many areas where future works can be done in future. The works for future study are discussed as follows.

In this work, the DC Characteristics i.e. I-V characteristics and transconductance are calculated from the quasi-2D modeling but the high frequency parameters such as cut-off frequency and maximum power output are not calculated. These parameters are very essential for the performance evolution of the device at high frequencies and they are required to examine in future.

The total current in the channel for different bias conditions are determined which is extremely exciting but the breakdown voltage is not determined, which is a vital limiting parameter of device performance. Further work can be extended to determine the breakdown voltage.

All simulations were based on drift-diffusion modeling of the transport characteristics. This model assumes full-ionization, non-degenerate, steady-state and constant temperature. In particular, the drift-diffusion approach cannot reproduce velocity overshoot and often overestimates the impact ionization generation rates. Hydrodynamic simulation, which considers self-heating effects and velocity overshoot of the carriers, should be performed for submicron gate DHEMTs for high frequency operation. Another interesting aspect is thermal simulation. In the simulation scheme used in this study, the isothermal condition is applied throughout the calculations. However, thermal effects are pronounced in the fabricated DHEMTs due to the low thermal conductivity of the sapphire substrate. Using the hydrothermal simulation, the heat generation in each part of the device can be simulated and can be accounted for in the design of the device later on. Moreover, InGaN/InN/InGaN double heterostructures should be further studied using a better simulation scheme that includes the latest III-Nitride material parameters for InGaN as the understanding of this material system improved considerably over the last few years.

Accurate modeling of the device is the first step for accurate Monolithic Microwave Integrated Circuits (MMIC) design. Therefore, accurate large signal modeling is necessary for future studies of power amplifiers with InGaN/InN/InGaN DHEMTs.

## References

- [1] Y. C. Kong, Y. D. Zheng, C. H. Zhou, Y. Z. Deng, "A novel  $\text{In}_x\text{Ga}_{1-x}\text{N}/\text{InN}$  heterostructure field-effect transistor with extremely high two-dimensional electron gas sheet density," *Solid-State Electronics*, vol. 49, pp. 199, (2005).
- [2] R. Chu, Y. Zhou, J. Liu, D. Wang, K. J. Chen, K. M. Lau, "AlGa<sub>N</sub>-Ga<sub>N</sub> Double-Channel HEMTs," *IEEE Transactions on Electron Devices*, vol. 52, no. 4, April, (2005).
- [3] M. S. Islam, S. M. Muhtadi, M. T. Hasan, A. G. Bhuiyan, M. R. Islam, A. Hashimoto and A. Yamamoto, "AlInN/InN metal oxide semiconductor heterostructure field effect transistor," *Phys. Status Solidi (C)*, vol. 7, No. 7-8, pp. 1983-1987 (2010).
- [4] C. Q. Chen, J. P. Zhang, V. adivarahan, A. Koudymov, H. Fatima, G. Simin, J. Yang and M. Asif khan, "AlGa<sub>N</sub>/Ga<sub>N</sub>/AlGa<sub>N</sub> double heterostructure for high power III-N field effect transistors," *Applied Physics Lett.*, vol. 82, no. 25, 23 June, (2003).
- [5] Quan Si, Hao Yue, Ma Xiaohua, Zheng Pengtian, and Xie Yuanbin, "AlGa<sub>N</sub>/Ga<sub>N</sub> double-channel HEMT," *Journal of Semiconductors*, vol.31, no.4, April (2010).



## Appendix A

### List of the Values of Different Parameters of InN Semiconductor

<b>Crystal structure</b>	Wurtzite
Density ( $\text{gcm}^{-3}$ )	6.81-6.89
<b>Dielectric constant</b>	
Static	15
high frequency	6.7-8.4
Lattice constants ( $\text{\AA}^\circ$ )	a = 3.54 c = 5.70
Optical phonon energy (meV)	73
<b>Band structure</b>	
Energy gap (eV)	0.7
Deformation Potential (V)	7.1
InN/GaN Conduction band discontinuity (eV)	0.45
InN/GaN Valance band discontinuity, (eV)	1.05
Effective Conduction band density of states ( $\text{cm}^{-3}$ )	$9 \times 10^{17}$
Effective Valance band density of states ( $\text{cm}^{-3}$ )	$5.3 \times 10^{19}$
<b>Ionization energy of donor</b>	
Donor level of N vacancies $V_N$ (meV)	40-50
<b>Valence band</b>	
Effective electron mass (in units of $m_0$ )	0.11
Effective hole mass [heavy] (in units of $m_0$ )	1.63

## Publications List

### Reviewed Journal:

- [1] **Md Rejvi Kaysir**, Md. Rafiqul Islam, "Theoretical Charge Control Investigations in InN-Based Quantum Well Double Heterostructure High Electron Mobility Transistors (QW-DHEMTs)", *Advanced Materials Research (AMR) Journal*, Vol. 403-408, pp. 52-58, November, 2011.
- [2] Md. Tanvir Hassan, **Md. Rejvi Kaysir**, Md. Sherajul Islam, Md. Rafiqul Islam and Ashraful G. Bhuiyan, Akio Yamamoto, "2DEG properties in InGaN/InN/InGaN-based double channel HEMTs", *Physica Status Solidi (C)*, Vol. 7, No. 7-8, pp.1997-2000, 2010.

### International Conference:

- [1] **Md Rejvi Kaysir**, Md Rafiqul Islam, "Theoretical Charge Control Investigations in InN-Based Quantum Well Double Heterostructure High Electron Mobility Transistors (QW-DHEMTs)", *Proceedings of 7<sup>th</sup> International Conference on MEMS, NANO and Smart Systems (ICMENS 2011)*, Kuala Lumpur, Malaysia, 4-6 November, 2011.
- [2] Md. Tanvir Hassan, **Md. Rejvi Kaysir**, Md. Sherajul Islam, Md. Rafiqul Islam, Ashraful G. Bhuiyan and Akio Yamamoto, "2DEG properties in InGaN/InN/InGaN-based double channel HEMTs", *Proceedings of 8<sup>th</sup> International Conference on Nitride Semiconductor (ICNS-8)*, Vol-1, P-792, Jeju, Korea, 18-23 October, 2009.